1

DNA Nanoengineering and DNA-Driven Nanoparticle Assembly

Alain Estève and Carole Rossi

University of Toulouse, LAAS-CNRS, 7 avenue du colonel Roche, Toulouse 31031, France

1.1 Introduction

In much the same way as the use of silicon did in the 1970s, leading to the modern information technology industry, the development of advanced functional nanomaterials will fuel many of the emerging industries that will address energy, healthcare, and environmental challenges as well as those in other areas. Therefore, a current challenge in the field of nanotechnology and materials science is the development of strategies to control the structuring and fabrication of functional materials and devices with potentially atomic scale precision on a large length scale, i.e. up to microscale and even centimeter scale. These new advanced functional materials aim at improving performances and developing new functionalities.

Traditional miniaturization approaches, classically referred to as "top-down" approaches, are derived from the microelectronics industry. These methods are primarily dedicated to semiconductor materials and are currently based on powerful and efficient techniques for structuring matter that are essentially operated by standard and industrial machines. These top-down technologies face a number of issues, including cost and the need for machinery modifications and manufacturing lines to promote miniaturization and mass production. Importantly, these technologies also face the intrinsic physical limitations inherent to the miniaturization of classical materials, which necessitates fundamental modifications to the overall device architecture. For instance, the concept of planar metal–oxide–semiconductor (MOS) transistor was proposed and developed since the mid-1960s and is one reference of the road mapping in microelectronics [1].

Self-assembly and, at large scales, "bottom-up" technologies are game changers in the way that materials can be envisaged. Along with the era of nanotechnology launched in the United States in the 1990s, the inspiration from the living world, where the directed assembly of molecules allows the production of organisms, was a disruptive technological alternative [2, 3]. If we compare the dimensions of the devices reachable by the "top-down" technologies to those of the living world

Biological Soft Matter: Fundamentals, Properties, and Applications, First Edition.
Edited by Corinne Nardin and Helmut Schlaad.

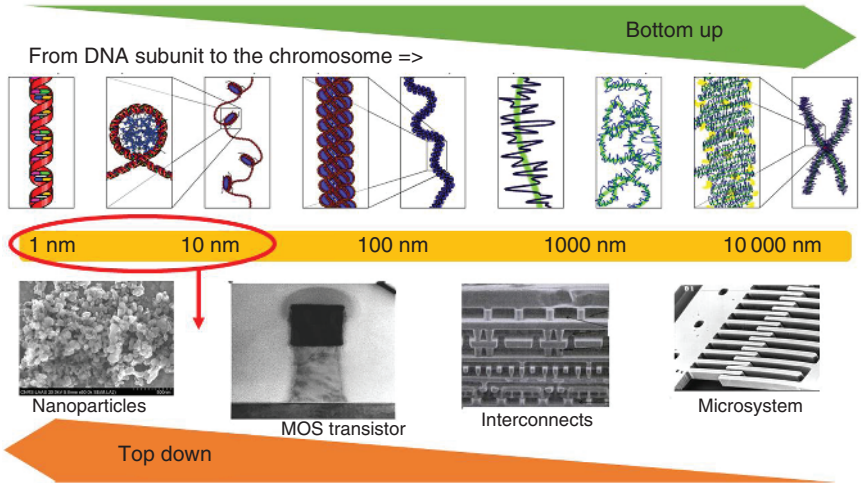

Figure 1.1 Perspective of the relative scaling of the synthetic and biological worlds with respect to multiscale DNA architecture.

(see Figure 1.1), two technological paths emerge that may lead to a refoundation of the classical concepts of technologies in favor of systems that are highly heterogeneous in chemical and structural nature.

To date, numerous bottom-up strategies have been investigated [4, 5]. These approaches fully rely on self-assembly, which consists of using the basic physical and chemical attractive/repulsive interactions (van der Waals, electrostatic, hydrogen, or covalent bonding) as well as the basic processes of molecular recognition in biology. The goal of these strategies is to interface and link various nano-objects, such as nanoparticles (NPs), nanotubes, biological molecules, and other organic objects [6], without external intervention.

Among these self-assembly strategies, a particularly interesting and versatile technique is to take advantage of the exquisite properties of deoxyribonucleic acid (DNA), i.e. the permutations and complementarity of nucleotide sequences, to program and direct the assembly of nano-objects in potentially extremely complex architectures, which is not feasible by any other state-of-the-art technique. This idea was first proposed in 1982 in the seminal work by Nadrian Seeman [7], who proposed the construction of nanometric "tiles" from elementary DNA bricks and to build regular networks of tiles for the formation of larger two-dimensional (2D) or three-dimensional (3D) structures.

This initial revolutionary concept to deviate from the original biological function of DNA and use it as a versatile and programmable technological brick was rapidly extended in many different directions [8]. More complex hybrid structures were produced by combining DNA with other materials (inorganic or not) while also taking full advantage of the recognition capability of folded DNA, so-called aptamers, and, finally, of modified DNA strands (chemical terminations, for peptide nucleic acid [PNA]) to extend its ability to combine other materials and fabrication techniques [9].

These studies led to a technologically wide and active field of study called DNA nanotechnology in which DNA is considered to be an engineering material that can be used as an architectural material, functional building blocks, and devices for applications not strictly dedicated to biology – in other words, a field in which DNA is no more utilized as the carrier of the genetic information in the cell [10]. The use of DNA out of its biological context is now widely accepted by the scientific community, which has been accompanied by the massive industrial production of artificial DNA. This concept opens unparalleled perspectives for the nanoengineering of a multitude of "new advanced materials" for various applications such as energy, environment, health, etc. [11–13]

In 2017, there were 400 published articles (source: Web of Science) on DNA nanotechnology in high-impact journals. Section 1.2 will give a brief overview on the DNA biomolecule and its primary features and properties, which will be followed by a description of the founding studies on DNA nanotechnologies in Section 1.3. Then, Sections 1.4 and 1.5 will focus on nanoparticle DNA-directed assembly, accompanied with state-of-the-art techniques and a case study by the authors on Al/CuO assembly. DNA nanotechnologies can be split into two fields:

- *DNA nanostructures (Section* 1.3*)*. As proposed by Nadrian Seeman [7], relatively small DNA strands are assembled to constitute elementary "bricks," which can be further used to fabricate larger structures that essentially comprise DNA and have one, two, or even three dimensions. The folding of much longer strands, such as the genome of the M13 virus, with the help of DNA staples (short DNA strands having partitioned complementarity with the longer DNA strand) is another way of generating structures any shape one can imagine [14]. Notably, small-sized DNA strands can also fold into specific conformations, making it possible to have very specific interactions of the lock and key type, as proteins typically do in biology. These DNA strands are called aptamers [15].
- *DNA as technological tool to drive nanoparticle assembly*. DNA can be used as a "cement" to guide in the self-assembly of various organic and nonorganic nano-objects. This pathway, directly inspired by the work of Nadrian C. Seeman, was first demonstrated in 1996 by Chad A. Mirkin who implemented the directed assembly of gold nanoparticles by DNA strands [16]. This research field has become very active, accounting for approximately 10% of all published articles on DNA nanotechnology over the past five years (source: Web of Science), whereas it represented less than 1% in the 2000s. A wide variety of different building-block shapes and different strategies for assembling them have been reported thus far, as summarized in Section 1.5. To date, nanoparticle and colloidal particle assemblies using synthetic DNA have allowed for the production of mostly plasmonic, photonic, or phononic metamaterials.

Interestingly, another new application of DNA nanotechnologies is the synthesis of highly ordered metal/oxide nanoparticle structures for energy-generating materials. The properties of these materials, also called nanothermites, are highly dependent on the size of nanoparticles and their distribution in the 3D structure. In this context, the use of DNA strands to direct self-assembly shows great potential

for the synthesis of nanothermites with outstanding energetic performances. Section 1.5 focuses on the nanoengineering of DNA to self-assemble Al/CuO nanothermite to illustrate the potential of DNA nanotechnologies in obtaining high-performance nanothermite for practical applications.

1.2 From the DNA Molecule to Nanotechnologies

DNA is a core constituent of all living cells, containing the genetic information from which all the functions of an organism are programmed. The composition and properties of DNA have been extensively studied, and the DNA double helix is certainly one of the best-known structures in biology. DNA is composed of sequences of nucleotides that are themselves made up of three components (Figure 1.2): a phosphate group bonded to a sugar (deoxyribose) to which a nitrogenous base is linked. It is therefore a true modular framework consisting of sugars and phosphate groups as a backbone that can harbor one of four different nitrogenous bases, including adenine (A), thymine (T), cytosine (C), and guanine (G), ensuring the sequential signature of the DNA molecule as well as the complementarity required to form the double helix.

The nitrogenous bases are complementary, where adenine (A) and guanine (G) can specifically interact with thymine (T) and cytosine (C), respectively, due to hydrogen bonds (two for the first "couple" and three for the second). Hybridization is the pairing of two complementary single-stranded DNA sequences, which results in the formation of a double helix. The energy gain resulting from the association of two single strands of DNA is, in the first approximation, the sum of the association energies of each pair of base pairs, with 2 and 3 k_BT (where k_BT is the thermal stirring energy) for A-T and G-C, respectively. Note that hybridization is a complex process characterized by the interplay of mutual attractive forces, including hydrogen bonds, solvent, and counterions to screen the negatively charged backbone.

The four primary characteristics that make DNA an excellent technological brick for nanoconstruction are the following:

- Reversible Watson–Crick pairing, which is based on the complex interplay between the solvent, DNA backbone, and hydrogen bonds, including interbase hydrogen bonds. External stimuli such as the temperature, pH, or ionic strength of the solution can denature the DNA double helix, where it is separated into its single-strand components. In addition, DNA can be repaired by DNA modification enzymes, particularly ligases. This specificity is especially used for the nanoconstruction of complex DNA patterns.
- Its size is ideally suited to nanoconstruction. The diameter of the double helix is approximately 2 nm, the distance between bases is 0.34 nm, and the helical pitch is composed of 10.5 bp, which corresponds to approximately 3.5 nm.
- The stability and flexibility of an assembly can be adjusted. The persistence length of double-stranded DNA is ~50 nm (or 150 bp). Below this length, the strand can

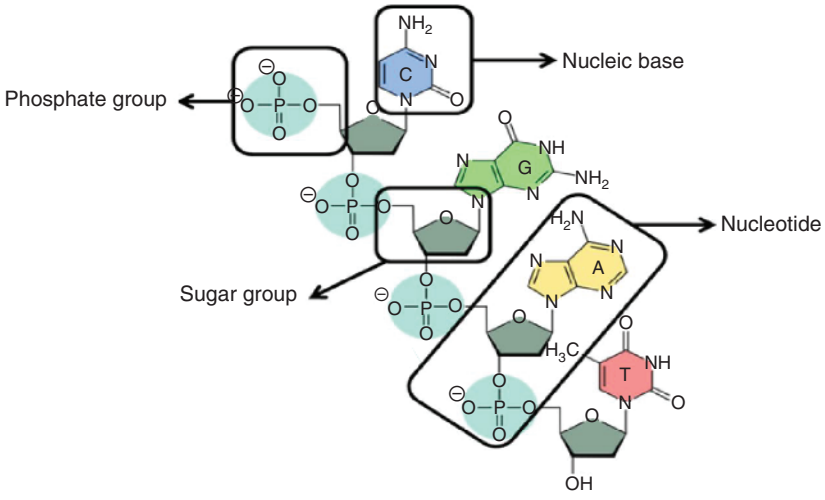

Figure 1.2 Schematic of the DNA molecular substructure.

be considered as a rigid rod, whereas it becomes very flexible beyond this length. There is also a difference in flexibility between double- and single-stranded DNA, with the latter being much more flexible, with a persistence length of only 1 nm, allowing for the formation of true loops or curved structures.

- Finally, 50 years of molecular biology research on DNA has produced a consistent palette of tools for DNA synthesis, manipulation, and modification. Many companies specifically offer synthetic DNA with a great variety of chemical modifications. It is now possible to order or create, in the laboratory, single or double DNA strands consisting of the desired nitrogenous base sequence with a wide variety of chemical or biological functions that can be further integrated at the strand termination or at a specific locations within the strand.

In addition to the remarkable intrinsic properties of DNA, all of these features lay the foundation for important expectations regarding DNA nanotechnologies to control the structuring and fabrication of functional materials and devices. The following examples shall illustrate the implementation of these technologies.

1.3 DNA Nanostructures: From Holliday Junctions to 3D Origami

As mentioned earlier, the development of DNA nanotechnologies began with the seminal work by Nadrian Seeman in the 1980s [7]. He envisaged associating several double strands of DNA with the help of the hybridization of so-called "sticky ends" to build more complex DNA networks. "Sticky ends" refers to as DNA terminations that remain single stranded, offering hybridization possibilities with other basic DNA elements with complementary single-stranded termination.

In doing so, he faced a number of issues due to DNA helices being highly flexible, and the resulting assemblies did not exhibit the desired structural stability. To address this problem, the Seeman team came up with the idea of building complex structures of branched DNA, strands called "tiles," the simplest configuration of which was called DX (for double crossover; Figure 1.3). These structures are highly rigid owing to their double points of attachment and four points of external sticky-end attachments. They were the first building blocks used for the construction of more complex networks based on DNA, and the first 2D networks were created by his team in 1998 [20].

Several studies followed based on these DX structures (Figure 1.3) [17, 21, 22], giving rise to more complex structures, such as TX-type tiles (triple crossover) [23–25] and PX type (paranemic crossover) [26, 27].

In the mid-2000s, another key step in the emergence of DNA nanotechnology was the development of DNA origami by Paul Rothemund [14]. This breakthrough concept significantly increased the complexity, versatility, and size of DNA structures.

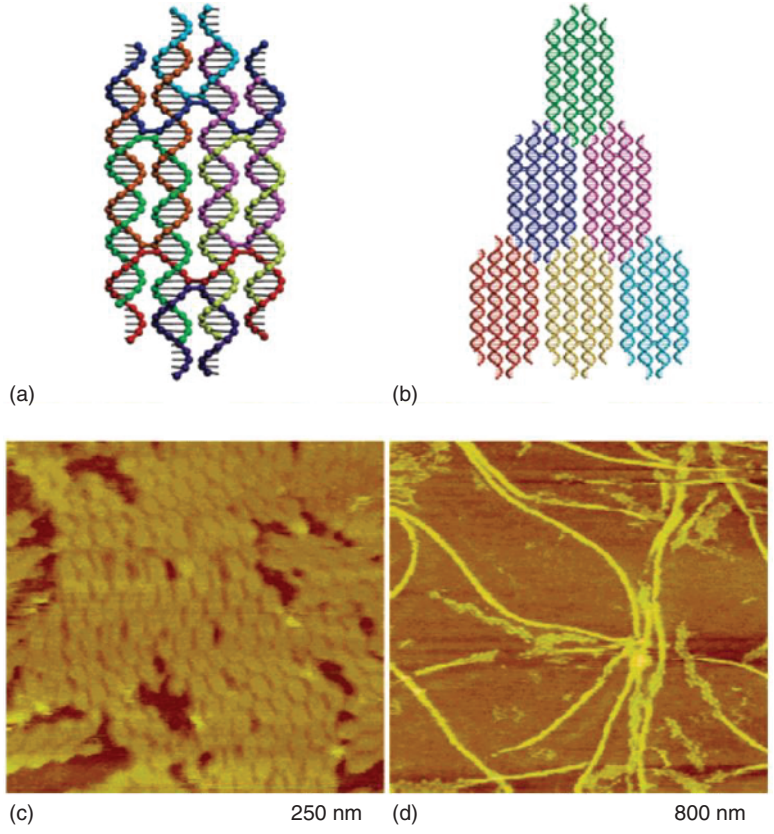

Figure 1.3 DX DNA-based structure (a,b) and AFM image of a 2D crystal made of branched DX motifs (c,d). Source: Reprinted with permission from Reishus et al. [17]. © 2005 American Chemical Society.

The term "origami" refers to the Japanese art of making various unique 3D forms with a paper sheet through folding techniques. In DNA origami, the paper sheet is a long DNA strand (obtained from DNA extraction of the M13 virus), which can be considered to be a scaffold that is folded into the desired shape by means of hundreds of small oligonucleotides (see Figure 1.4a) called "staples." Each staple is designed to bind to different locations of the long strand to induce local folding, which collectively cause the overall DNA strand to acquire a defined shape. Rothemund illustrated the versatility of this concept by creating a number of different structures (Figure 1.4b). A key advantage of this technology is that it is not necessary to precisely control the stoichiometry and purification of oligonucleotides, because the use of a long scaffold makes the assembly highly selective. The minimum of

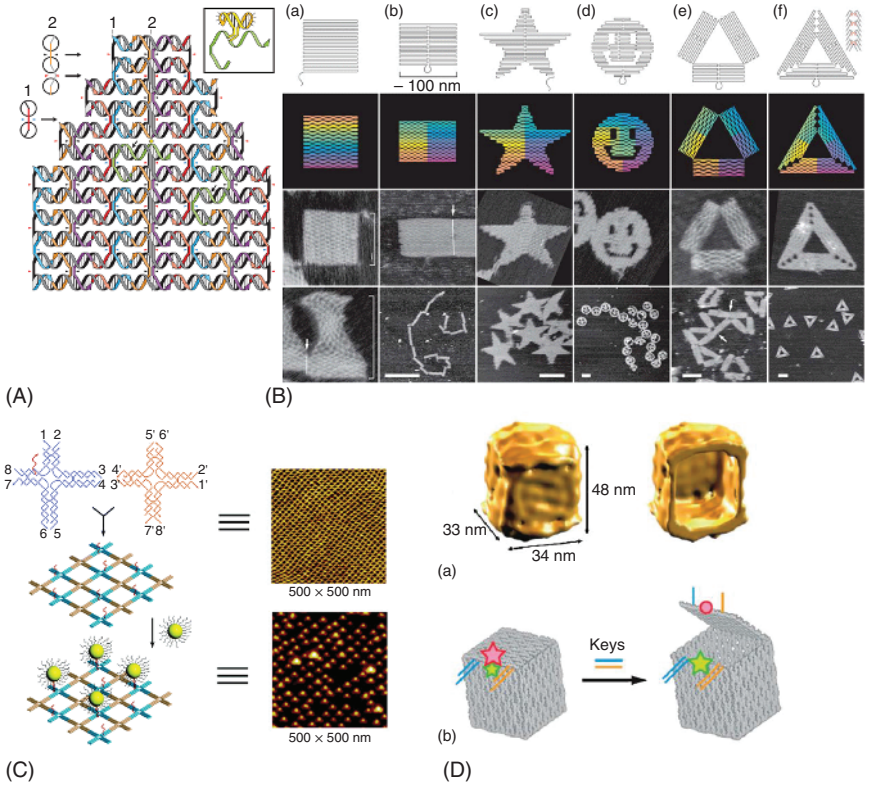

Figure 1.4 (A) Design of a DNA origami. Source: Reprinted with permission from Rothemund [14]. (B) Different shapes obtained using the origami technique: (a) square; (b) rectangle; (c) star; (d) smiley; (e) and (f) triangles. The first two lines correspond to design images from computer simulation, while the two other lines correspond to experimental validations. Source: Reprinted with permission from Rothemund [14]. (C) DNA nanostructures used as templates for the assembly of a 2D network of gold nanoparticles. Source: Reprinted with permission from Zhang et al. [18]. (D) Full origami DNA box. The box may be actuated for closing/opening through the introduction of an oligonucleotide. (a) Reconstructed from transmission electron cryomicroscopy experiment, and (b) is a schematic of the origami box. Source: Reprinted with permission from Andersen et al. [19].

energy is reached when all the staples are associated, regardless of the number of staples by unit volume. DNA origami achieved immediate success, thanks to the overall reliability in reproducing complex 2D and 3D shapes and its conceptual and experimental simplicity. The progress in this technique has resulted in the formation and control of uniform structures with unprecedented complexity.

Importantly, this method is associated with an automated computer design strategy. Indeed, all DNA folding and associated staples must have their base sequences designed depending on each other and must be preprogramed with the help of computer-aided design procedures. Therefore, the staples are determined before the manufacturing of origami and ordered from DNA synthesis companies.

In addition, DNA staples can be obtained with chemical or biological modifications, the subtle positioning of which within the origami structure can yield a chemically or biologically functional structure. Similarly, by including thiol termination at specific locations of the origami, Zhang et al. managed to create a periodic network of gold nanoparticles on a DNA-modified surface (Figure 1.4c) [18].

After numerous studies and publications on 2D DNA origami, the concept has been extended to 3D DNA origami [19], which appeared for the first time in 2009. The Gothelf and Kjems teams at the Center for DNA Nanotechnology (CDNA) at the University of Aarhus in Denmark demonstrated the connection of several 2D origami planar structures at their edges. In their report, they described in detail the formation and characterization of a DNA box with a controllable lid (Figure 1.4d). Two sides of the box were hinged to one side and held closed along the opposite edge by a pair of "staple" DNA strands called "locks." Each lock can be opened by adding a DNA strand complementary to the strands constituting the locks to the solution, releasing the lid of the DNA box.

In summary, since the initial vision of Seeman in the early 1980s, fundamental steps in the programming and engineering of DNA nanostructures have succeeded one another, and the invention of the DNA origami technique has allowed for the considerable development of these technologies, making it possible to create complex structures with any shape and precise properties. However, it is important to note that production yields tend to fall as soon as the complexity and density of structures increases. Furthermore, the lack of detailed information on the folding process remains an obstacle to the development of DNA nanotechnologies. Thus, extensive studies on the fundamental thermodynamic versus kinetic aspects of the folding processes should be pursued.

1.4 DNA-Directed Assembly of Particles: From Concepts to the Realization of Ordered Assemblies

An interest in using DNA nanotechnology to program the assembly of nanoparticles and colloids into larger hierarchical structures emerged in the 1990s (Alivisatos et al. [28] and Mirkin et al. [16]). Using the controlled chemistry of sulfur on gold surfaces, both groups had the idea of grafting single-ended thiol-terminated DNA strands (–SH) onto gold nanoparticles.

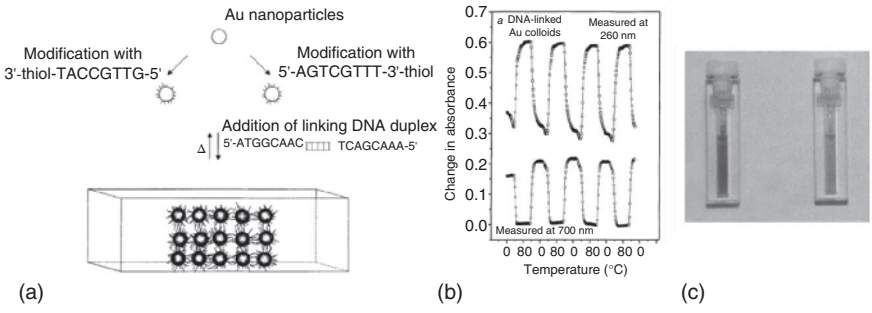

Figure 1.5 (a) Schematic diagram of the linker self-assembly of 13-nm-diameter gold nanoparticles (left figure). (b) Measuring the absorbance at 260 and 700 nm of the colloidal solution of nanoparticles as a function of temperature (0 and 80 °C) and demonstrating the reversibility of the hybridization of the DNA strands. (c) Image of the colloidal solution heated to 80 °C (red) and cooled to 0 °C (blue). Source: Reprinted with permission from Mirkin et al. [16]. © 1996 Springer Nature.

The Mirkin team made use of thiol-modified oligonucleotides (–SH) at one end of the strand for chemical grafting onto the surface of 13-nm gold nanoparticles [16]. Two separate solutions of gold NPs modified with noncomplementary strands were made and mixed in equal amounts. A single-stranded DNA sequence that was complementary to both strands was then added in excess to the above mixture. This additional DNA strand acted as a "linker" and induced the assembly of the nanoparticles into aggregates of several microns by hybridization of the linker strands with both strands grafted onto the nanoparticles. The color of the nanoparticle solution gradually changes from pink (dispersed particles) to blue (aggregated particles). An interesting aspect of this type of assembly is its reversibility. Indeed, at ∼55 °C (the so-called melting temperature), dehybridization of the strands takes place, and the redispersion of the nanoparticles causes the solution to return to its initial pink color (see Figure 1.5). Alivisatos chose to work on particles that were 10-times smaller, onto which a single oligonucleotide sequence was covalently attached using alternating strand with distinct sequences. Then, hybridization was performed at different defined positions of a long single strand that resulted in the nanoscale-controlled positioning of the NPs along the one-dimensional (1D) DNA strand. Undoubtedly, the controlled interplay of complementary and noncomplementary DNA strands makes DNA nanotechnology one of the most powerful bottom-up approaches for building hierarchical architectures of nano-objects (noble metals, semiconductors, oxides, and polymers) with an almost infinite variety of high-performance programmable DNA/nanoparticle hybrid materials. Since the seminal work by Alivisatos and Mirkin on gold nanoparticles, many DNA/nanoparticle assembly processes have been reported mostly by varying the DNA length and processing conditions and to generate materials for applications in biodiagnostics [8–11], therapeutic agents [12, 13], plasmon-enhanced spectroscopy [14–16, 20, 29], magneto-optical sensors [17], catalysis [21] and energetic materials, which will be presented in detail in Section 1.5.

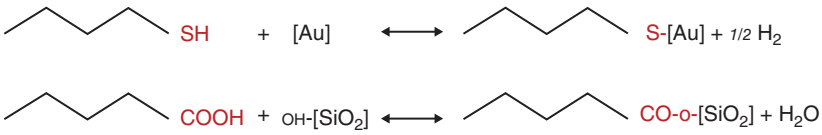

Figure 1.6 Typical thiol-terminated species for a gold surface (in brackets) chemical reaction (top chemical reaction equation) and carboxylic acid (COOH)-terminated species to a hydroxylated (OH) silicon dioxide surface (in brackets) chemical reaction (bottom equation). Source: Based on Vericat et al. [30].

1.4.1 DNA/Nanoparticle Assembly: Primary Functionalization Strategies

The most successful and widespread technique for gold surface functionalization technique used to graft DNA strands uses thiol chemistry, taking advantage of the well-known and controlled reaction between thiol and metal surfaces (such as gold; see Figure 1.6) [30]. An alternative method using antigen/antibody interactions has been reported to immobilize DNA strands on surfaces, notably oxide surfaces [31], extending the possible applications of the organized and controlled heterogeneous structures of nanoparticles.

The biotin/streptavidin interaction is recognized as one of the strongest noncovalent interactions in nature, having a complex dissociation constant of 4×10^{-14} mol/l and a formation enthalpy of $30\,k_BT$ [32]. This strong interaction results from a perfectly adjusted protein pocket for biotin such that its binding is insensitive to pH, salinity, and temperature. Streptavidin is a protein consisting of four tetrameric fragments, each of which can accommodate four biotin species, which are immobilized onto streptavidin and form hydrogen electrostatic and hydrophobic bonds with the aromatic amine groups of streptavidin. The use of this interaction has attracted a great deal of interest because of its versatility, and it can be applied to any type of surface, even gold, provided that the surface is sufficiently reactive to ensure that the protein is immobilized. For example, Cobbe et al. proposed an aggregation of gold nanoparticles previously functionalized with a biotin group using streptavidin and single-stranded DNA [33]. The two strategies used in this study are schematically shown in Figure 1.7a,b, respectively. The self-assembly of heterogeneous nanoparticles by protein–DNA interactions and their differences from gold were also assayed by Oleg Gang and coworkers [34].

Finally, we should mention the use of other chemical functions, such as carboxylic acid (–COOH), which is more appropriate for metal oxide surfaces, or other oxides, such as silicon dioxide (see Figure 1.6). While the literature commonly reports on organic coatings to inhibit further oxidation of metallic nanoparticles, to the best of our knowledge, no mention of these possible chemical species has been addressed with respect to DNA.

1.4.2 Toward High-Order Crystalline Structures

In practice, the overall optimization process for controlling DNA-directed assembly in the liquid phase is a highly complex task. Over the last several decades, substantial

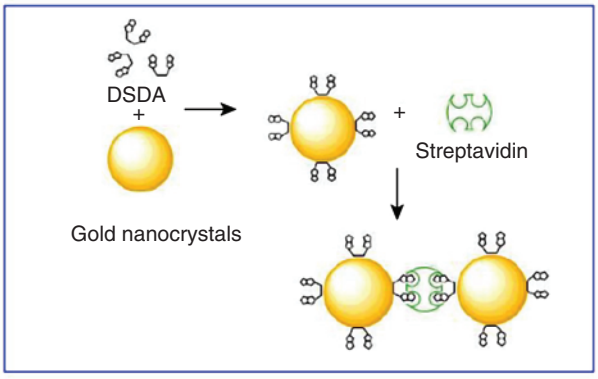

(a)

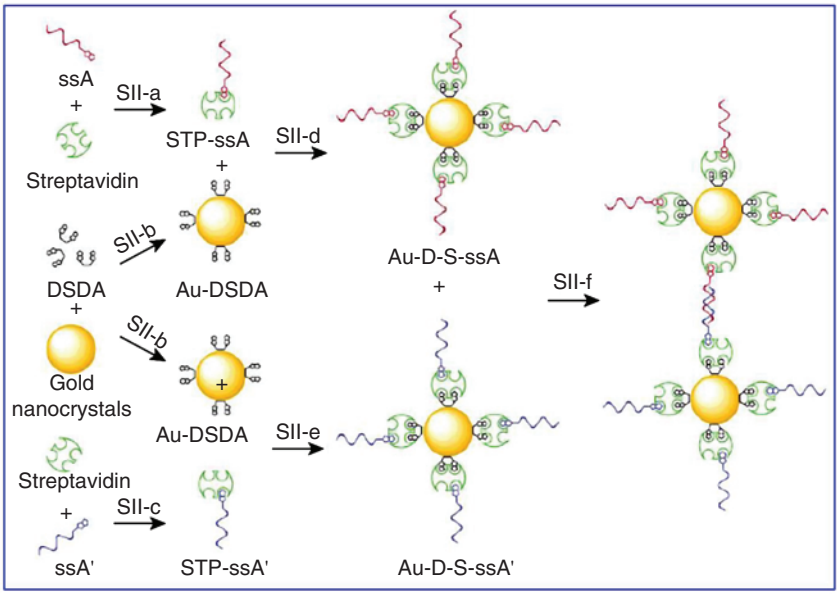

(b)

Figure 1.7 (a) Direct biotin/streptavidin-mediated nanoparticle aggregation. (b) Protocol for the biotin/streptavidin-mediated DNA-driven assembly of nanoparticles. Source: Cobbe et al. [33]. © 2003 American Chemical Society.

progress has been achieved in understanding and controlling the wet chemical technical parameters for the patterning of matter at the nanoscale, especially the effect of salt concentration on both the grafting density and hybridization of DNA strands [35–37] or the heterogeneity of DNA grafted on anisotropic nanoparticles as demonstrated very recently [38]. Highly ordered face-centered cubic (fcc) and body-centered cubic (bcc) structures of 5- or 10-nm gold nanoparticles have been described with different DNA strand lengths and a programmable interparticle distance (as illustrated in Figure 1.8) [39, 40] and have more recently been

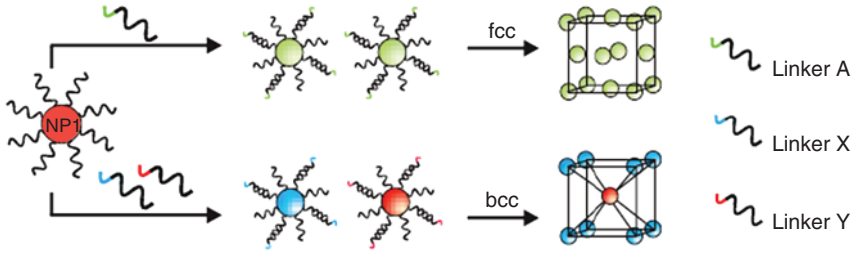

Figure 1.8 Diagram summarizing the influence of the linker on the crystalline structure obtained after the self-assembly of gold nanoparticles. Source: Park et al. [39]. © 2008 Springer Nature.

reported with the crystallization of nanoparticles into more complex structures (VB23, 24).

It is now known that several key parameters have a large effect on the assembly kinetics and architecture of the final structures:

- The ionic concentration in solution, such as the salt concentration (NaCl, $MgCl_2$, etc.). Park et al. have shown that the salt concentration tends to decrease the interparticle distance by decreasing the repulsive interactions between nanoparticles.
- The spacer nature of the oligonucleotide also influences the interparticle distance. Indeed, a "slump" of an oligonucleotide on the nanoparticle was observed with a spacer composed of repeated adenine bases, reducing the interparticle distance by 2.5-fold because of a greater affinity of this base with gold compared with that observed with other bases [41, 42].
- The DNA strand length impacts crystallinity, where an excessively long strand lowers crystallinity because nanoparticles are less constrained, whereas a short link with respect to the size of the nanoparticle does not allow crystallization due to the size polydispersity of nanoparticles [40, 43, 44]. Experimental phase diagrams showing the crystallinity of gold nanoparticles as a function of these parameters have been established [45]. Owing to the flexibility of their structure, DNA strands are also reprogrammable, allowing a crystal structure to be directly altered in solution by selecting the appropriate oligonucleotide sequence [46] or by introducing DNA interlayers, modifying the stiffness and temperature sensitivity of the DNA bond [47]. For example, Gang et al. recently determined gold nanoparticle phase diagrams based on stoichiometry (i.e. the relative proportion of two populations of gold nanoparticles with complementary DNA strands), the size of nanoparticles, and the length of DNA linker, both experimentally and theoretically, using coarse-grain models [48]. These phase diagrams are shown in Figure 1.9, where gold nanoparticles can adopt the crystal phase of CsCl, AlB_2, or Cr_3Si depending on the size of the nanoparticles or the linker.
- The temperature of the solvent also influences crystallinity. By aggregating at a temperature close to the melting temperature of DNA, a transition can take place at which nanoparticles are allowed to rearrange into well-defined crystalline structures and on a larger scale. Figure 1.10 shows the principles of

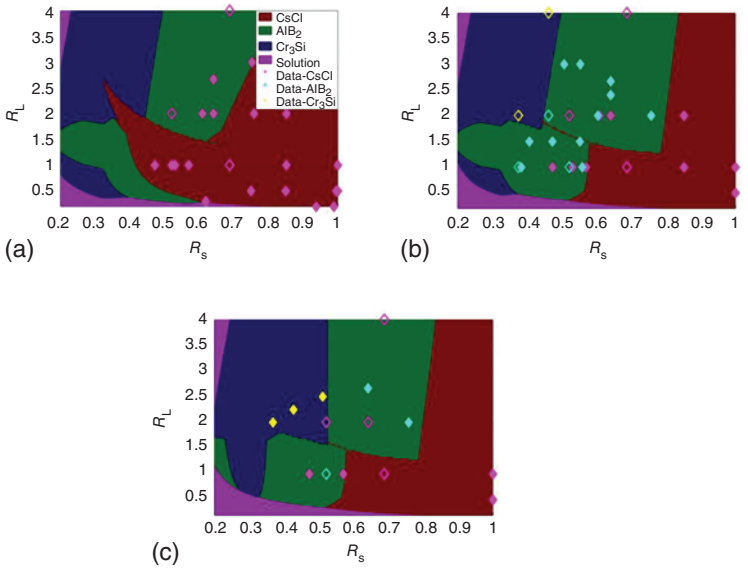

Figure 1.9 Gold nanoparticle phase diagrams as a function of nanoparticle size (RS) or linker length (RL) for three different stoichiometries (in a binary mixture, the ratio in terms of the population of nanoparticles functionalized with a given sequence versus another set of nanoparticles with the complementary sequence): (a) 1 : 1, (b) 2 : 1, and (c) 3 : 1. The symbols represent the experimental points: the solid symbols represent the pure structures, while the voids represent polymorphic structures. Overall, there is good agreement between experimental points and theoretical results [48].

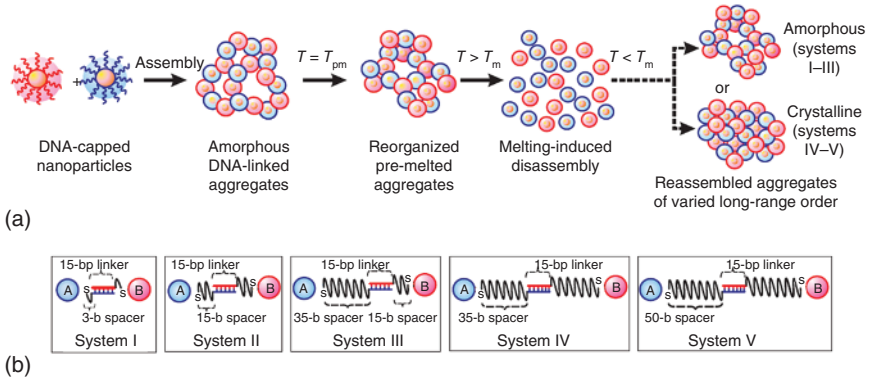

Figure 1.10 Diagram showing the behavior of nanoparticle aggregates formed upon DNA self-assembly versus (a) temperature and (b) the length of DNA strands used. Source: Nykypanchuk et al. [40]. © 2008 Springer Nature.

this rearrangement and gives the ingredients, thermal treatment, and spacer length required for obtaining crystals [40, 49, 50].

Thus, the quality of the crystallization is strongly dependent on the temperature conditions. Cooling the colloidal solution at a sufficiently slow rate, which can take from two to three days, was recently shown to lead to the formation of micrometric rhombic dodecahedron "super crystals." [51] In contrast, performing self-assembly at a constant temperature below the melting temperature results in the polycrystallization of the nanoparticles, which are then less organized despite having undergone the annealing process [52]. Importantly, the formation of these dodecahedra is independent of the size of nanoparticles, showing that this structure is thermodynamically the most stable that is achievable for such systems. Finally, post-crystallization modifications have also made it possible to increase the temperature ranges or solvents in which these structures can be used by adding organic complexes or encapsulating DNA in silica [52, 53]. Notably, it is also possible to control the number of functionalized strands on the surface of gold nanoparticles with one, two, or more strands by "sorting" a colloidal solution of nanoparticles by electrophoresis. This technique allows for the hybridization of two or three nanoparticles alone (dimers or trimers) that have optical properties dependent on the interparticle binding, which is governed by the nature of the DNA binding and can be dynamically altered in solution [46, 54] by ionic interactions and the chemical nature of the substrate [55]. Thus, the chemical nature of the surface of the gold nanoparticles depends on the ligands used to stabilize the colloids. Lermusiaux et al. investigated the optical properties of dimers immobilized on the surface of gold nanoparticles as a function of the ionic concentration and the hydrophobicity of the surfaces by varying the nature of the ligand. The results presented in Figure 1.11 show that the use of an amphiphilic ligand (i.e. having both a hydrophobic and hydrophilic group) makes it possible to improve stability in terms of decreasing the unwanted aggregation of nanoparticles or in the conformation between two assembled nanoparticles.

1.4.3 Crystallization of Heterogeneous Systems

The vast majority of work has focused on the self-assembly of gold or silver nanoparticles, owing to their good colloidal stability, controlled synthesis, and subsequent controlled thiol chemistry. However, extending their potential applications requires manipulating other materials. Gang et al. have proposed a general strategy of nanoparticle functionalization by DNA that is theoretically applicable for a wide range of materials [34], which they applied to three model materials: gold nanoparticles with palladium of three different shapes (cube, octahedron, and dodecahedron), iron oxide (Fe_2O_3), and quantum dots (CdSe/CdTe/ZnS and CdSe/ZnS). They identified three primary parameters that are crucial in establishing heterogeneous superstructures: (i) the role of the shape of the nanoparticle on crystallinity, (ii) the influence of nonspecific interactions related to the presence of DNA, and (iii) the emergence of disorder when manipulating multielemental

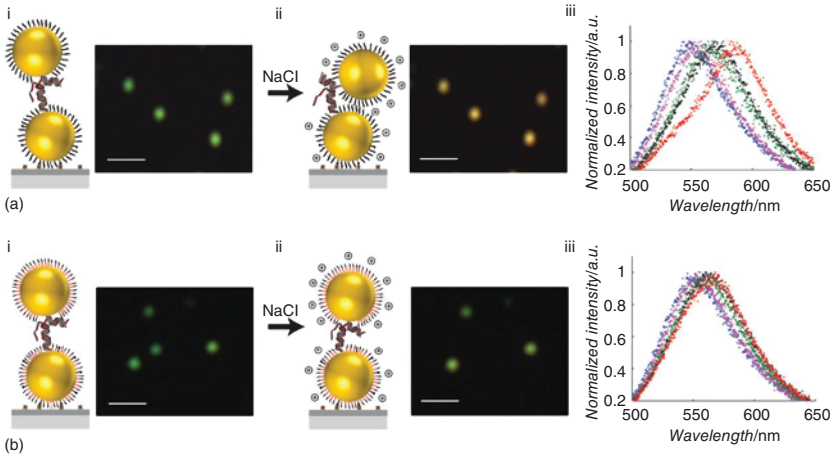

Figure 1.11 Comparison of the variation in the interparticle distance of 40-nm-diameter gold nanoparticles organized into dimers according to the use of hydrophilic (a) or amphiphilic (b) ligands for their stabilization after increases in the saline concentration (i, 5 mM NaCl; ii, 800 mM NaCl) by dark-field microscopy and (iii) spectral absorbance analysis. Source: Reprinted with permission from Lermusiaux and Bidault [55].

structures. This work follows the pioneering work by Severac et al., who first demonstrated the possibility of using DNA as an assembly vector in the context of the synthesis of high-energy-performance materials from Al and CuO nanoparticles [56]. In addition, Fan et al. developed assemblies of five nanoparticles of different sizes involving a small nanoparticle surrounded by four larger nanoparticles [57]. Such anisotropic assemblies have the advantage of having better defined optical properties. In addition, Tan et al. developed a general and simple single-step method for the functionalization and crystallization of anisotropic systems from two nanoparticle sizes [58]. Beyond the grafting densities that strongly change with anisotropy, a predominant effect of the nanoparticle curve, which is dependent on the size of the nanoparticle, has been observed [59, 60]. Jones et al. have studied the crystallization of nonspherical nano-objects, such as octahedra, prisms, and rods [61]. In general, the resulting structures of these objects remains the one that allows for the maximum hybridization of DNA strands [62] and involves a superposition of nanoprisms [63], a 1D arrangement of nanorods, or a classical crystallization in cubic face centered and cubic centered [61]. However, only small aggregates are obtained, and it remains difficult to obtain crystals on large scales. From a theoretical perspective, Travesset and Knorowski have studied the self-assembly of nanocubes [64], and a face-to-face orientation of the cubes was obtained when short strands were used, while several other structures could be obtained using longer DNA strands with application of osmotic constraints. Finally, Macfarlane et al. demonstrated the possibility of obtaining complex ternary systems by inserting a third size of nanoparticles into a preexisting binary structure (see Figure 1.12) [65]. This process has made it possible to establish a wide range of crystalline structures in a completely reversible manner owing to the use of DNA,

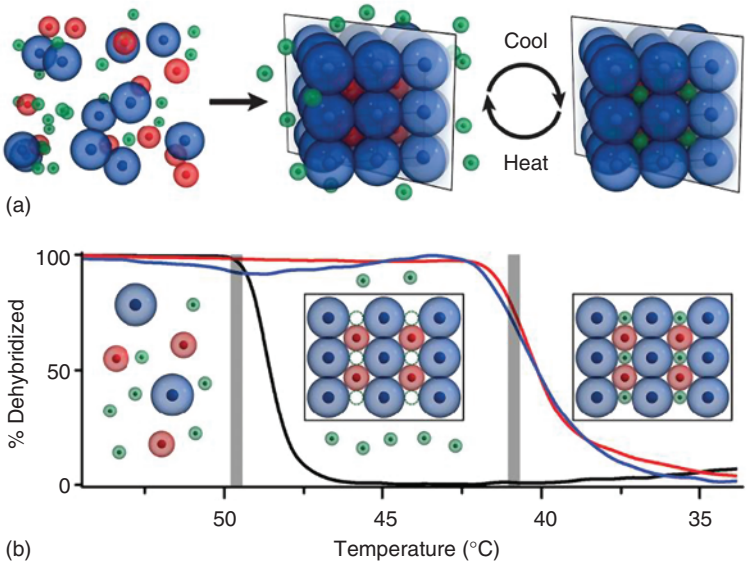

Figure 1.12 Diagram of the self-assembly of nanoparticles by DNA in ternary crystalline structures. A binary structure is first synthesized prior to insertion of a third size of nanoparticle into a predetermined site (a). In (b), the thermal analysis of the ternary structure is presented. Source: Macfarlane et al. [65]. © 2013 American Association for the Advancement of Science.

opening the way for the development of a method that can be generalized to other materials.

The previously described work primarily focuses on the aggregation of nanoparticles, the diameter of which can vary from 10 to 150 or even 200 nm. However, other teams have observed different behaviors using micrometer-sized nanoparticles, specifically with respect to their ability to stabilize colloidal solutions with increase in temperature. Indeed, interactions between particles vary with their size, especially with respect to weak van der Waals interactions that can lead to nonspecific and irreversible aggregation [66]. Therefore, crystallization is much more difficult to achieve, and the aggregates are amorphous gels with a fractal structure [66–68]. Crocker et al. demonstrated the possibility of crystallizing microspheres into short hexagonal crystals under extremely precise experimental conditions with respect to temperature and especially surface preparation [69–71]. Indeed, only a specific method of functionalization by swelling/deflating micrometric organic particles (such as polystyrene) immersed in organic solvent in the presence of polyethylene glycol (PEG) was successful [69]. Beyond this example, the phenomenon of reversibility with temperature is rarely observed and strongly depends on the length of the DNA bond and the temperature, which must be sufficient to dehybridize double-stranded DNA without irreversible aggregation of the nanoparticles. Although a recent review did not report significant progress in the self-assembly of micrometric particles [72], a team from the United States recently demonstrated the possibility of functionalizing micrometric organic particles (polystyrene or

poly(methyl methacrylate) [PMMA]) or inorganic (titanium oxide or silicon oxide) with single-stranded DNA by a generic method of alkyne–azide cycloaddition [73]. This method enables higher DNA grafting densities compared to methods making use of the biotin/streptavidin complex, consequently allowing for crystallization of the particles at room temperature or optimized rearrangement after annealing.

1.4.4 DNA/Nanoparticle Assembly: Applications

The most intriguing applications of DNA nanotechnology, those that best take advantage of the small size, biocompatibility, and programmability of DNA-based systems, lie at the interface with biology. Below, we highlight key successes in the development of DNA-based imaging probes for biomolecular detection and prototypes of smart therapeutics and drug delivery systems. Several dynamic plasmonic systems have also been demonstrated for applications in energy harvesting, nanophotonics, and imaging: [74]

Biomolecular detection. One of the first applications of DNA nanotechnology put into practice was biomolecular detection based on the colorimetric principle. For example, gold nanoparticles initially functionalized with complementary strands may be disintegrated in the presence of a target species, hybridizing with a portion of the DNA strands (see Figure 1.13) [75, 76]. Disintegration caused by the dehybridization of the two complementary strands is associated with a color change from blue to red in the colloidal solution. This principle has been used by many teams to detect several species, such as thrombin [77], adenosine and cocaine [75],

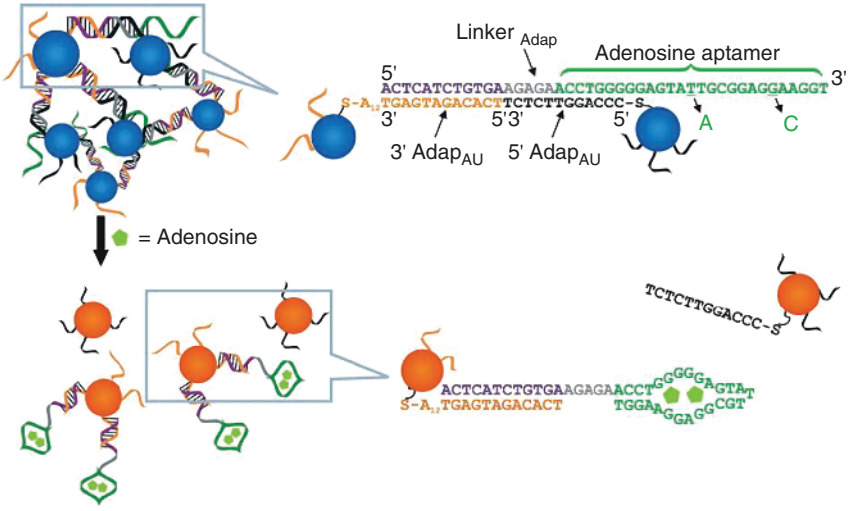

Figure 1.13 Schematic diagram of the detection of adenosine using the colorimetric method. Functionalized gold particles with DNA strands are aggregated owing to the presence of a complementary aptamer with adenosine. Thus, in the presence of the target molecule, the aptamer hybridizes to the molecule, causing particle de-aggregation and a colorimetric shift in the solution from blue to red [75].

or cysteine [76]. The possibilities are numerous but limited by the relatively high detection concentrations (in the nanomolar range) compared with the higher sensitivity that is attainable with fluorescence-based methods [78].

Optical and plasmonic devices. Crystals composed of specific inorganic and semiconductive nanoparticles, also called "quantum dots," have the advantage of having luminescence energies that have for biomedical applications replace the traditional organic fluorophores used for imaging, exhibiting lower luminescence and greater sensitivity to the spectrum of white light [79]. Their association with a metal such as gold allows for further increase in the photoluminescence released by the quantum dots. Thus, the organized assembly of gold nanoparticles and quantum dots allows the photoluminescence of the structure to be controlled according to several parameters, such as the size of the constituents and the interparticle distance, allowing for the monitoring of biological events and the development of improved plasmonic spectroscopies.

Catalysis. Finally, the control of the size, composition, and density of particles is crucial for catalysis, where DNA can provide novel possibilities. A drawback is that DNA requires a specific aqueous environment, limiting catalysis by passivating the surface of nanoparticles, making them less reactive. To overcome these difficulties, Auyeung et al. developed a three-step process where after synthesizing a superstructure of gold nanoparticles, they freeze the structure in the silica and then calcine the whole structure, resulting in an organized porous structure [80]. In summary, the authors predict a real utility for catalytic reactions using gold, such as the oxidation of alcohol or carbon monoxide or reduction via plasmonic effects.

1.5 Nanoengineering of DNA Self-Assembled Al/CuO Nanothermite

While much of the literature describes the DNA-directed assembly of gold nanoparticles, achieving the assembly of oxide nanoparticles is a technically complex task due to increased surface chemistry issues. This constitutes a formidable scientific challenge that well illustrates all possible routes to optimization of practical and efficient technological solutions and the promise of novel and practical applications in energy-generating materials. This last section is devoted to such an application example, i.e. applications associated with thermite energetic materials. Interestingly, we present a series of methodological steps that have been performed to visualize and optimize the DNA-directed assembly of Al and CuO nanoparticles, which can be generalized to many other materials.

Thermites are substances that store chemical energy that can be released after being submitted to an external electrical, optical, or pressure wave stimulus. These substances are composed of a fuel (most of the time aluminum) mixed with an oxidizer, which can be varied to monitor reaction properties. This metastable mixture undergoes exothermic oxidation/reduction reactions upon bonding of Al with O atoms. The aluminum/copper oxide (Al/CuO) system is among the most interesting

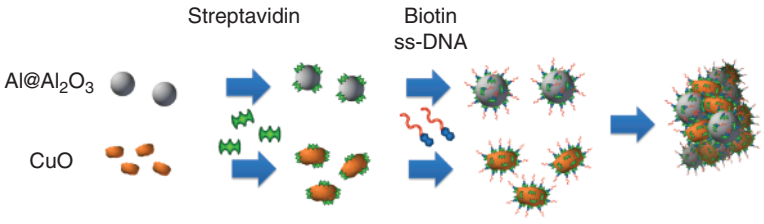

Figure 1.14 Illustration of the functionalization process developed to enable the DNA-directed self-assembly of core-shell Al (Al covered with Al_2O_3 shell) and CuO nanoparticles.

as it offers high energy density and reactivity, particularly when mixing Al and CuO nanoparticles, compared with their micronic counterpart. Energetic materials are used in widespread applications, including space, military, automotive, and civil security industries. In the early 1990s, taking advantage of Al and CuO compatibility with microelectromechanical systems (MEMS) fabrication techniques, we proposed their integration into silicon-based microsystems for the realization of local micro-actuations in extremely small volumes (less than a cubic millimeter) and relatively substantial forces (~0.1 N). In this context, DNA nanotechnologies open perspectives to create *ad hoc* materials that are high performance, safe, and are REACH legislation compatible [81–86]. The exothermic oxidation/reaction process, in which oxygen atoms are liberated from their CuO matrix (reduction until pure copper) to oxidize aluminum, with formation of alumina, can be represented by the following overall exothermic chemical reaction:

$$3CuO + 2Al \rightarrow 3Cu + Al_2O_3$$

The properties of these materials are highly dependent on the sizes of components and their distribution in the composite. The use of nanoparticles allows for a significant improvement of energetic properties, but there remain important issues with respect to controlling the mixing of nanoparticles at the nanoscale. In this context, the use of DNA self-assembly shows great potential for the synthesis of new types of nanothermites with exquisite control of the contact surfaces between oxidizer and reducer, thereby enabling the optimization and control of energetic performances.

Our approach to using DNA for the controlled assembly of Al and CuO NPs into thermite aggregates is outlined in Figure 1.14.

In the following section, we will successively detail and discuss the following: (i) the fundaments and characterization of DNA interactions and overall grafting protocol, (ii) the characterization of DNA-directed assembly, and (iii) the performances of DNA-assembled Al/CuO energetic nanomaterials compared with those of nanopowder mixtures.

1.5.1 Fundaments and Characterization of DNA/Surface Chemistry and Grafting Strategies

To guide technological steps, we provided an atomic scale understanding of intrinsic physical and chemical interactions taking place between DNA and oxide surfaces.

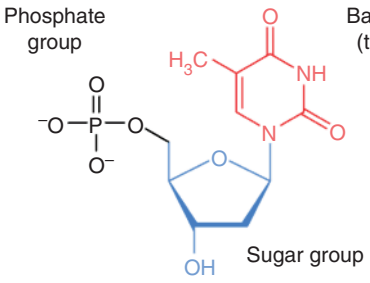

Figure 1.15 Schematic of the dTMP molecule with its subunits equivalent to those of DNA.

To allow for experimental and atomic scale simulations of synergistic associations, we proposed to use a representative *dTMP* molecule that includes all DNA subunits instead of a full DNA fragment (*dTMP*: 2-desoxi-thymidine-5′-monophosphate). Then, we studied the chemical interaction of *dTMP* molecules with controlled alumina surfaces through X-ray photoelectron spectroscopy (XPS) and infrared spectroscopy. The experimental results were supported by density functional theory (DFT) calculations. In a second stage, we developed, characterized, and optimized the overall grafting protocol by quantifying all processing steps.

1.5.1.1 DNA/Alumina Interaction Evaluation Through Infrared Spectroscopy and First Principles Calculations

The *dTMP* molecule, as shown in Figure 1.15, is a rather small molecule compared with DNA strands with multiple bases. However, it still harbors all DNA subunits, including a phosphate group, a sugar, and a base. The alumina oxide surface is chosen as it is much simpler to manipulate and characterize at the atomic scale than CuO. Notably, to provide well-controlled model surfaces, we used flat alumina surfaces deposited by atomic layer deposition (ALD), which allows the thickness of alumina to be adjusted at the monolayer level.

We performed first-principles calculations to evaluate the different possible chemical reactions taking place at surfaces, which was one of the objectives of the quantification of all *dTMP* vibrational modes of the different and most pertinent configurations (either in the liquid or in contact with the surface) for assignation of the complex infrared IR spectra obtained experimentally. One such calculation is shown in Figure 1.16, corresponding to the most stable configuration of all trials, indicating chemical reactions at both the phosphate and base sites, with an energy gain in the order of 1–2 eV compared with *dTMP* in the liquid phase [87].

Based on theoretical calculations, we first experimentally validated the irreversible nature of the interaction of *dTMP* with alumina. After performing rinsing and ultra-vacuum pumping steps, XPS measurements clearly indicated the presence of *dTMP* on the surface, as shown in Figure 1.17. The results showed the appearance of nitrogen and phosphorus signals, demonstrating the presence of DNA. A detailed analysis of these spectra with respect to the influence of the initial dTMP concentration indicates a chaotic and/or multilayered coverage, as well as the quantification of carbon extra-contamination that probably results from the overall deposition procedure (ALD, *dTMP*, and rinsing).

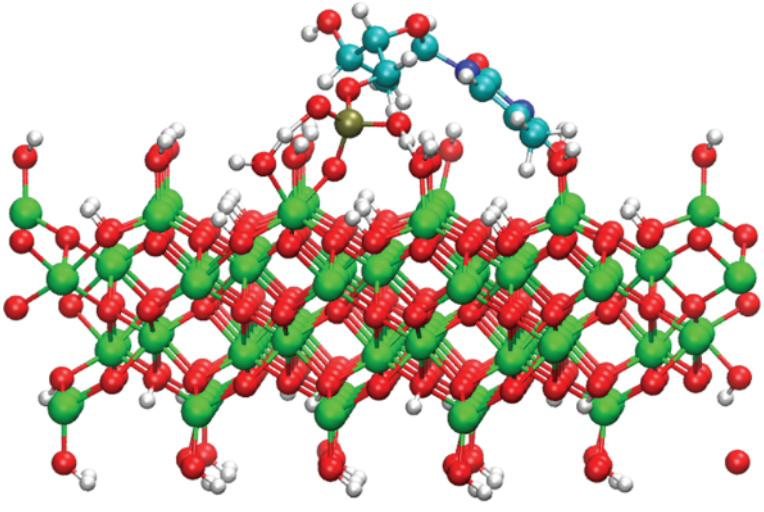

Figure 1.16 Chemisorption of dTMP on a hydrated Al_2O_3 surface (with an –OH termination) in the most stable case, i.e. with formation of covalent bonds at the level of phosphate and thymine groups [87].

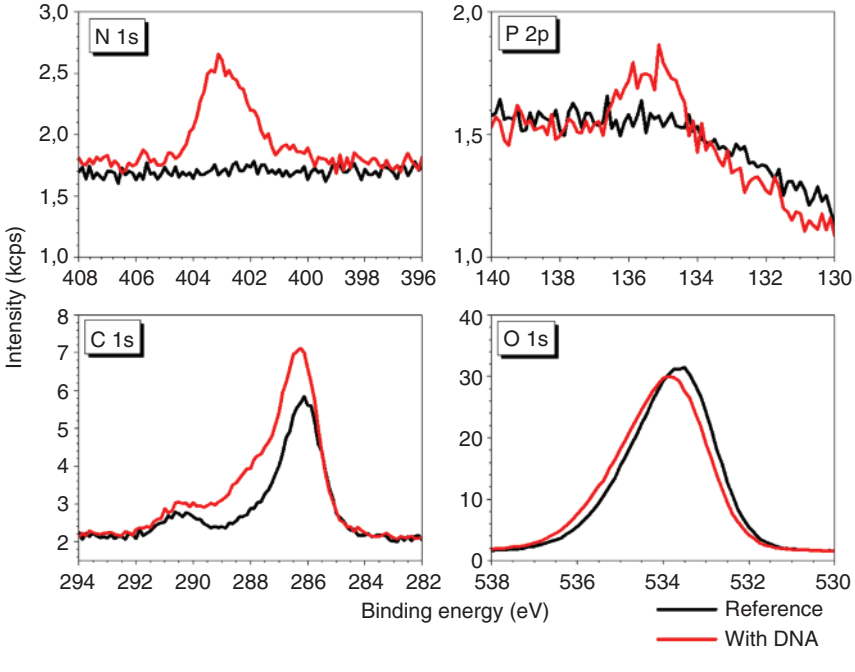

Figure 1.17 XPS spectra for three primary elements in dTMP deposited on alumina surface. The black curve corresponds to the signal of the reference (alumina substrate), while the red curve corresponds to the alumina surface with deposited dTMP [87].

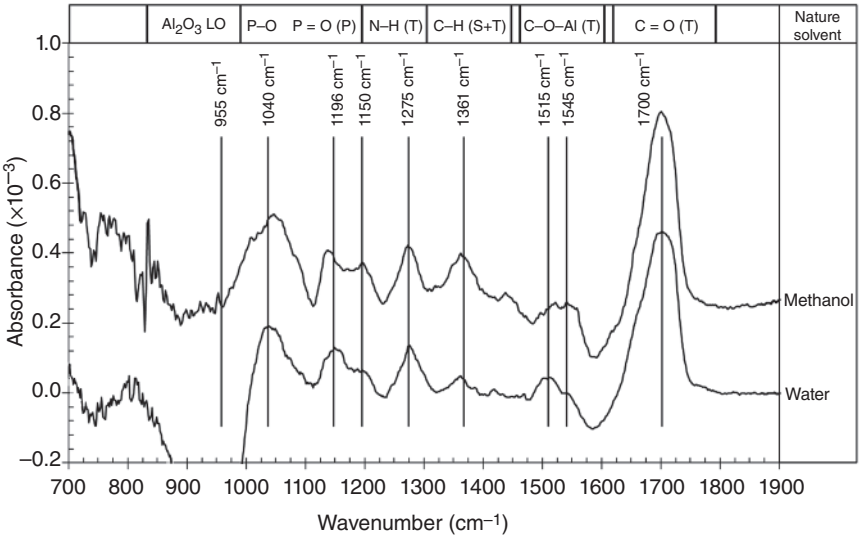

Figure 1.18 Influence of the nature of the solvent on the IR absorbance spectra of an alumina surface after dTMP deposition. The incubation of the surface was performed using methanol (top curve) and water (bottom curve) with the same concentration of dTMP to a clean alumina substrate in both cases. Related dTMP regions are reported on the top of the figure: T for thymine, S for sugar, and P for phosphate according to assignments resulting from DFT calculations [87].

To identify the bonding nature of *dTMP* with the alumina surface, we made use of infrared spectroscopy and extensively investigated deposition under multiple conditions (concentration, temperature, nature of solvent, etc.). Using first-principles quantification of vibrational modes to assign different and reproducible peaks, we confirmed the creation of covalent bonds and multiple interactions on the surface, particularly through phosphate and thymine dissociation. Such assigned spectra are shown in Figure 1.18, in which the nature of the solvent was modified (water and methanol).

To direct the assembly of Al and CuO, we decided to use a biotin/streptavidin grafting protocol. With the knowledge that direct, irreversible, and chaotic bonding would take place between DNA and alumina or CuO nanoparticle surfaces, screening them as much as possible through streptavidin coverage would lead to subsequent specific interaction of the antigen/antibody type with biotin-terminated DNA strands. In Section 1.5.1.2, we will describe this grafting protocol and the process of generating the Al and CuO colloidal solutions.

1.5.1.2 Functionalization Protocol and Colloidal Characterization

The overall DNA functionalization procedure, which is conceptually equivalent for both the Al and CuO nanoparticles, is shown in Figure 1.14. The first step of the process consists of the dispersion and stabilization of Al and CuO nanopowder. For the experiment, we used 15 mg of 50-nm CuO and 80-nm Al nanopowders of nominal size as provided by the suppliers. These nanoparticles were dispersed in

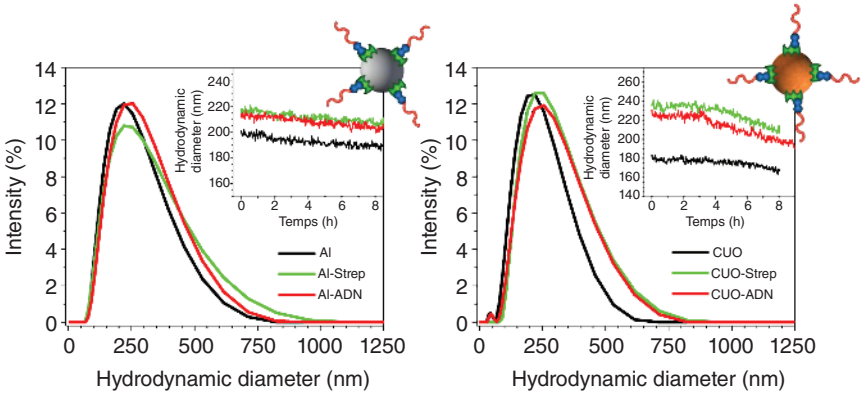

Figure 1.19 Schematic overview of primary DNA grafting steps and strategy for the Al/CuO directed assembly.

ultrapure deionized water containing a surfactant, Tween 20 (or polyoxyethylene (20) sorbitan monolaurate), which acts as a stabilizing agent, and the solutions were buffered to neutral pH (pH = 7). Tween 20 is a molecule comprising hydrophilic and hydrophobic regions on opposing sides. In solution with nanoparticles, these molecules nonspecifically interact with nanoparticles and prevent aggregation. During their dissolution, nanopowders do not spontaneously disperse, yielding numerous large aggregates, necessitating an ultrasound step followed by a sedimentation step. The solutions were ultrasonicated for eight minutes at 200 W while maintaining the temperature below 40 °C. The resulting solutions were then left overnight at room temperature, allowing large aggregates that have not been broken down to settle. The supernatant of the solutions is then recovered and characterized by dynamic light scattering (DLS). The results obtained for unmodified particles can be seen in Figure 1.19 (black curves). We observed hydrodynamic diameters (ZH) values of $\sim 224 \pm 7$ and 187 ± 5 nm for Al and CuO, respectively. Scanning electron microscopy results revealed that these colloidal solutions are composed of small indivisible aggregates of two to four nanoparticles, with diameters that are stable over hours. Note that a shell layer of approximately 3 nm of oxide covers the pure Al core of the Al nanoparticles. This protective shell allows the particles to remain unoxidized and stable in solution under neutral pH conditions.

Then, the grafting of streptavidin was performed after determining the optimal quantity that can be generated, which is derived from the total nanoparticle surface available in solution, considering a sphere approximation and knowing that streptavidin covers approximately 5 nm [2]. Finally, for both Al and CuO colloidal solutions, an excess of streptavidin was added. In both cases, an incubation time of at least four hours was used, and the solutions were rinsed multiple times to remove the excess of ungrafted streptavidin. Between each rinsing step, the solution was centrifuged and further dispersed in an ultrasonic bath after changing the solvent. Rinsing was performed out in a 0.1% diluted phosphate-buffered saline (PBS) solution containing 0.05 vol% Tween 20, although the grafting of streptavidin tends to

stabilize the colloids. Again, DLS measurements were performed, shown as green curves in Figure 1.19, and could be compared to ungrafted particle diameters. We observed a slight increase in the mean diameters due to the addition of streptavidin molecules. Notably, for the CuO nanoparticles, the inflation was more pronounced, which could be attributed to undesired interparticle interactions mediated by streptavidin or their accumulation in multiple layers.

The next step was to achieve biotin-terminated DNA grafting, owing to the biotin/streptavidin interaction. For streptavidin, the first step was to estimate the amount of DNA needed to functionalize all the available proteins on the surface of the nanoparticles. For both colloidal solutions of Al and CuO streptavidin-functionalized particles, which were previously prepared, we added the DNA solution at a concentration that was fivefold the amount necessary for the biotin-terminated DNA to complement the optimal surface density of streptavidin sites. Again, after incubation, rinsing, and centrifugation to remove excess DNA in solution, the colloidal solution was redispersed after each centrifugation in an aqueous solution of $0.1 \times$ PBS and 0.05% Tween 20 in an ultrasonic bath. Subsequently, the hydrodynamic diameter and zeta potential of the obtained functionalized nanoparticles were characterized by DLS. Results are shown in Figure 1.19 (red curves, obtained with 30-base DNA strands). Shorter (15 bases) and longer (45 bases) DNA strands have also been used, showing coherent results for CuO nanoparticles.

1.5.1.3 Quantification of Streptavidin and DNA Surface Densities

Based on previous fluorescence-based methodologies that were exclusively used for quantifying the grafting of DNA strands on gold nanoparticles, we have derived the following quantification strategy, which allows measurements of streptavidin and DNA surface densities [31, 88]. The end of the subsection describes the quantification of the grafted DNA that is still functional for hybridization, which we called the "hybridization efficiency." Note that in this section, hybridization is performed with DNA strands that are nanoparticle-free. Because of the permanent immobilization of streptavidin on the nanoparticle surfaces, we developed a method for quantifying the amount of streptavidin grafted onto Al or CuO. This process was performed in three steps (shown schematically in Figure 1.20) that quantify a. streptavidin coverage, (b) DNA coverage, and (c) hybridization efficiency, respectively, which are the primary principles detailed in the following section. For more technical details, see Calais et al. [31]:

Quantification of streptavidin surface density. Cy3-labeled streptavidin was added to the colloidal suspensions. After incubation, the solutions were centrifuged, and the fraction of unbound streptavidin (Figure 1.20a) was measured in the supernatant. The difference in the streptavidin concentration before and after centrifugation was used to deduce the amount of bound streptavidin, which was then normalized by the quantity of nanoparticles determined by atomic absorption spectrometry (AAS).

Quantification of DNA surface density. Fluorescent FAM oligonucleotides were added to Cuo^{Strep} and Al^{Strep} colloidal suspensions. After incubation, the

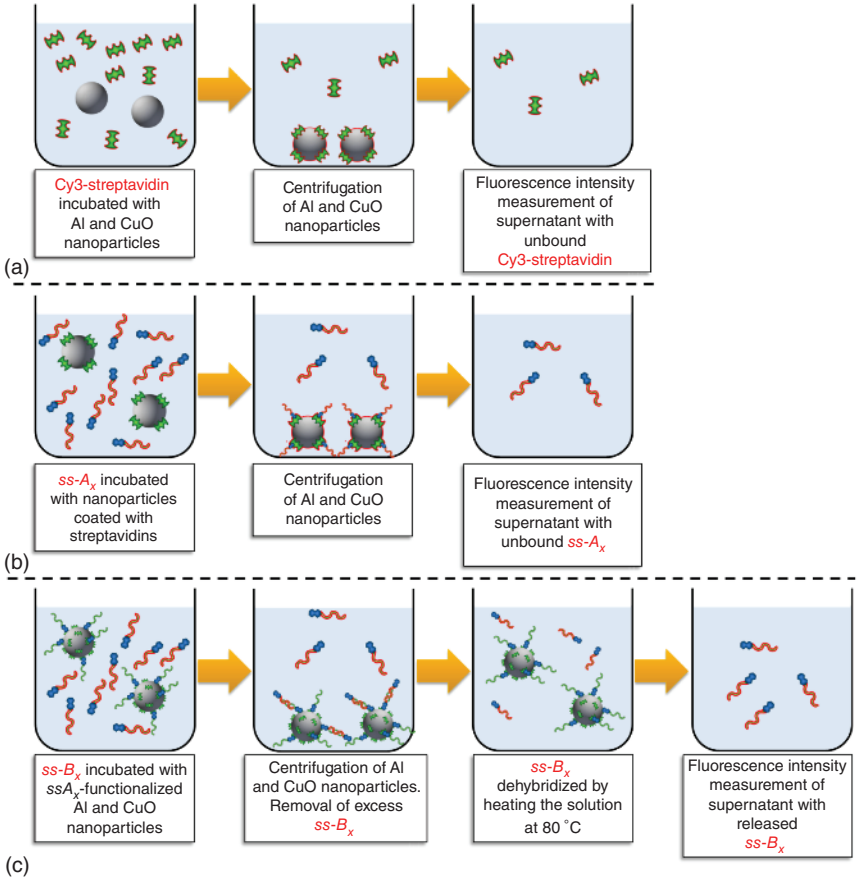

Figure 1.20 Schematic representation of the process developed for the determination of (a) streptavidin surface density on CuO or Al nanoparticles. (b) The DNA surface density on CuO or Al nanoparticles, and (c) the hybridization efficiency on CuO or Al nanoparticles.

solutions were centrifuged, and the fluorescence intensity of the supernatant was measured. The quantity of DNA grafted onto the nanoparticles was then determined from the difference between the initial DNA concentration (using a control sample) and the DNA concentration in the supernatant, which was then normalized by the quantity of nanoparticles determined using AAS. This protocol is summarized in Figure 1.20b. Note that the reversibility of the streptavidin/biotin interaction can be evaluated by heating/cooling the solutions containing functionalized Al and CuO nanoparticles.

Quantification of DNA hybridization efficiency. FAM-labeled oligonucleotides were added to Al and CuO colloidal suspensions previously functionalized with non-fluorescent strands. The NaCl concentration was set to enable the hybridization of the FAM-labeled strands with the nonfluorescent ones, grafted on the Al and CuO nanoparticles. After a few hours, the colloids were centrifuged and resuspended in solution (0.1 × PBS, 0.05% Tween 20, and NaCl) to remove excess DNA

Table 1.1 Quantification of streptavidin coverage, grafted DNA, and hybridization efficiency during the assembly protocol.

	Al			CuO		
Streptavidin coverage	$10 \pm 2\%$			$22 \pm 2\%$		
	Al			CuO		
	Grafted	*Hybridized*	*(%)*	*Grafted*	*Hybridized*	*(%)*
ADN per NP	6000	550	9%	25 000	1200	5%
	±1000	±80	(±3%)	±3000	±100	(±1%)
Without streptavidine	16 000	410	2.5%	30 000	760	2%
	±2000	±10	(±2%)	±8000	±60	(±2%)

strands. After rinsing, the solutions were finally heated to 80 °C for five minutes to dehybridize DNA double strands. The fluorescence intensity of the supernatant containing the released fluorescent strands was then measured, and the quantity of DNA strands grafted on the nanoparticles was calculated (see Figure 1.20c).

Overall, the results indicate that a careful handling of selected process parameters is required to maximize the DNA surface density. Particularly, we observe that 15–30-mM NaCl is required to avoid irreversible nanoparticle aggregation and that gentle sonication during the early stage of streptavidin incubation allows for increased streptavidin loading by approximately 175% and 135% for the CuO and Al nanoparticles, respectively. The DNA strand length has no noticeable impact on the DNA grafting density. We showed that direct grafting of DNA onto Al and CuO nanoparticles largely dominates the overall functionalization process, with DNA immobilization on streptavidin sites representing less than 5–10% of all DNA strands (see Table 1.1). As streptavidin covers only a small portion of the Al and CuO nanoparticle surfaces, a large surface area is prone to nonspecific interactions with DNA. We experimentally confirmed the strong chemical affinity of DNA bases with both copper oxide and alumina surfaces and the lack of control of the conformation of the immobilized strands onto the oxide surfaces. The higher density of grafted DNA observed for CuO suggests a partially spread-out conformation compared with the completely spread-out strands on Al. Finally, we quantitatively proved the crucial role of the antigen/antibody protocol to preserve the ability of DNA to hybridize, improving the hybridization efficiency by twofold, ensured by the specific DNA strands grafting onto streptavidin sites (~1.2 and 0.9 strands by streptavidin for CuO and Al nanoparticles, respectively).

1.5.2 Kinetics of DNA-Directed Assembly of Al and CuO Nanoparticles

Many parameters (length and nature of the spacer, NaCl concentration, etc.) clearly affect the assembly and crystallinity of nanoparticle aggregates. However, the role of

the coding sequence selected to enable hybridization upon aggregation has hardly been addressed, despite being a crucial factor in determining the thermodynamics and kinetics of aggregation. Various hybridization strategies involving strands of variable coding sequences have been described in the literature. In addition, the role of the length of the spacer has been investigated. However, the choice of the oligonucleotide sequence exclusively follows *a priori* empirical design and has not been studied nor commented on in an extensive manner. In this section, we propose to design and optimize the sequence that will be used to obtain our energetic nanobiocomposites *in silico*, which will be validated experimentally in a second stage. These results were published in Calais et al. [89].

1.5.2.1 Design and Impact of the DNA Coding Sequence

Referring to the pioneering research by Oleg Gang and coauthors [34], presenting a generic method for the functionalization of different types of nanoparticles (gold, palladium, iron oxide, or quantum dots), the chosen DNA strand is composed of a repeated T-base spacer to separate the coding portion that will be further hybridized to the surface of the particle, with a coding portion of 15 bases. A close examination of the sequence allowed us to notice that partial hybridization between two complementary strands was possible due to the repetition of the four AGGT bases twice in the sequence (AAT-AGG-TGA-AGG-TTA). In addition, folding of the strand on itself is possible when the spacer is composed of T bases, where the sequence becomes [(T)12-TTT-AAT-AGG-TGA-AGG-TTA]. This possible folding is crucial because it could prevent any hybridization with the complementary strand. In addition, this folding can result in "stranded" interactions when a large number of strands of identical composition are in solution. These parasitic interactions are schematically shown in Figure 1.21 and should be avoided or minimized.

Given the limited number of studies on the generation of an optimized DNA strand sequence of a length close to standard requirements, we have developed an algorithm to define an optimized sequence by removing four types of undesired interactions:

- The generated DNA strand must not fold back on itself to maintain its coding specificity.
- Noncomplementarity of the strand, total or partial, with a strand of identical composition. Based on the use of the DNA strand in solution, it is indeed inevitable to identify many identical strands capable of interacting with each other.
- The considered strand must hybridize over the entire coding portion of the other strand to better control the hybridization process.
- The fourth type of constraints is based on the definition of hybridization criteria, where the user first chooses to consider the minimum number of adjacent bases allowing for hybridization (denoted NM) (d), with the possibility of including one or two noncomplementary bases (f) between these adjacent bases. The value of NM is set to three by default, according to the Gibbs energies reported in the literature [90].

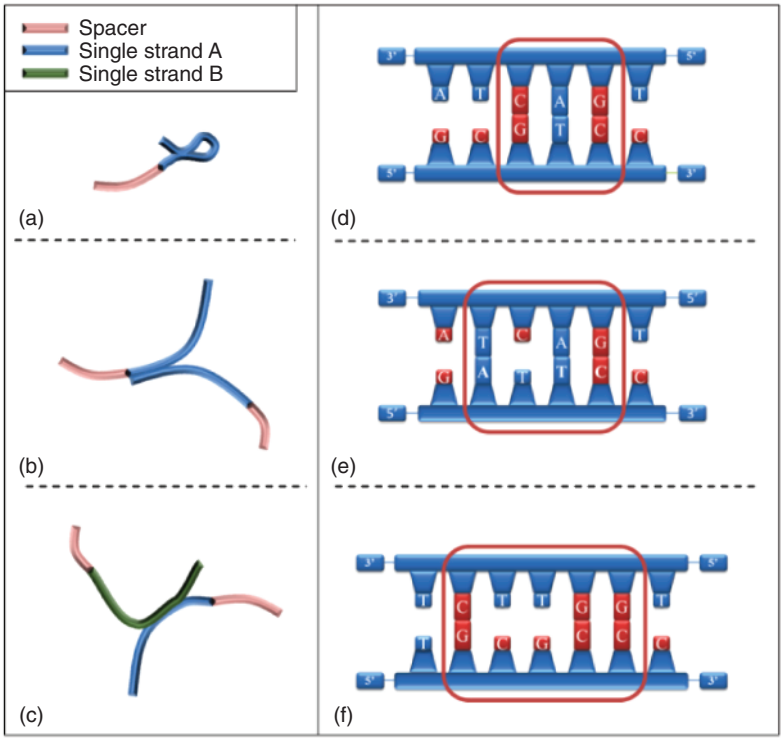

Figure 1.21 Schematic of the constraints used in the program. Oligonucleotides are represented by bars: red bars correspond to spacers (for example, repeated thymine bases), blue bars correspond to the sequence designed by the algorithm, and green bars correspond to the complementary strand of the designed oligonucleotide. (a) Avoidance of self-interactions for a single strand through the folding process, (b) hindered interactions (total or partial hybridization) between two strands with the same sequences, and (c) undesired partial hybridization of sticky-end sequences in the presence of their complementary counterpart. (d, e) Detailed and local sequence constraint: (d) a maximum of three adjacent bases are allowed to hybridize, and (e, f) mismatched sequences (noted as M) are forbidden when considering interactions [89].

Note also that constraint (b) is more restrictive than constraint (a) because it does not require a loop for hybridization such that the application of constraint (b) includes constraint (a). Considering all restrictions, the number of solutions drastically decreases from the intrinsic combination of DNA coding possibilities, which is tractable by computer analysis. The full details of our algorithm and obtained sequences are available in [89]. This optimization process allows the sequences to be selected according to the type of constraint applied and for the results to be sorted according to the melting temperature of each selected DNA strand. Such calculation results are shown in Figure 1.22a,c. For each sequence length, the table presents the best sequence in term of melting temperature that also fits the restriction requirements. The curve (a) of Figure 1.22 shows the number of available sequences for each DNA strand length that the operator wishes to implement in

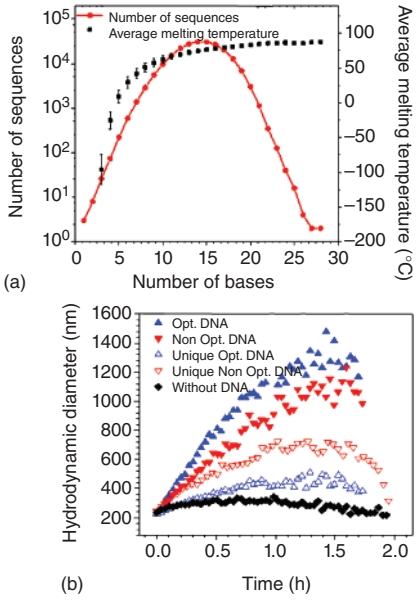

Number of sequences	Sequence	Melting temperature
4	GCGA	1 °C
5	CCG CA	28 °C
6	CCG CAC	42 °C
…	…	…
14	ACG GCA CCT CGC TT	85 °C
15	AGC GGA TGC CTT GGA	86 °C
…	…	…
27	CCT AAT GTA TCG CAG AGT TGA CGG GCT	87 °C
28	GGT AAT CTA TGC GAC ACT TCA GCC CGT T	88 °C

(c)

Figure 1.22 (a) Number of sequences obtained according to the number of bases by considering three adjacent bases necessary for the hybridization and the stresses (b, e of Figure 1.20) with the inclusion of noncomplementary bases between the three adjacent bases (red curve). (b) Evolution of the hydrodynamic diameter of Al-CuO aggregates: nonfunctionalized nanoparticles (black curve), functionalized with complementary optimized strands ssA-Opt and ssB-Opt (solid blue symbols) and noncomplementary ssA-Opt (empty blue symbols), and functionalized with strands with complementary non-optimized strands ssA-Lit and ssB-Lit (solid red symbols) and noncomplementary ssA-Lit (empty red symbols). (c) Partial list of optimized sequences with lengths from 4 to 28 bases obtained after ranking sequences according to their melting temperatures. These sequences take into account a spacer consisting of 7T bases.

the assembly protocol and the associated average melting temperature. Note that while melting temperature continuously increases, it starts to become saturated at a nominal level for a DNA length of approximately 6–10 bases.

To show to the importance of properly selecting the coding sequence of DNA strands, we compared the kinetics of aggregation of five different mixtures of Al and CuO nanoparticles performed under the same experimental conditions (see Figure 1.22 (b)) using an NaCl concentration of 35 mM at 25 °C:

- Aggregation between functionalized Al and CuO nanoparticles with complementary and optimized strands (solid blue symbols).
- Aggregation between functionalized Al and CuO nanoparticles with nonoptimized complementary strands (solid red symbols).
- Aggregation between functionalized Al and CuO nanoparticles with optimized but identical strands, supposedly noncomplementary (empty blue symbols).
- Aggregation between functionalized Al and CuO nanoparticles with optimized and identical strands, assumed to be noncomplementary (empty red symbols).

- Aggregation between nonfunctionalized Al and CuO nanoparticles, i.e. without a strand of DNA or streptavidin on the surface (black symbols).

First, no or little aggregation was observed between nonfunctionalized Al and CuO nanoparticles (black curve). Therefore, this experiment enables the absence of nonspecific interactions between particles to be verified under these conditions. Next, functionalized Al and CuO nanoparticles with identical strands, supposedly noncomplementary, are shown as blue and red empty symbols, respectively. While a lack of aggregation is expected, an increase in the hydrodynamic diameter is observed over time in both cases that is greater than that shown in the black curve, corresponding to nonfunctionalized Al and CuO particles. When the sequence of the DNA strands used has been optimized (blue curve), the increase of the hydrodynamic diameter is limited, reaching 500 nm after 1 hour 30 minutes. In contrast, when the DNA strands have not been optimized (red curve), the hydrodynamic diameter reaches 725 nm after one hour. In both cases, the aggregation is caused by nonspecific interactions between nanoparticles functionalized with DNA. These interactions may result from various factors that can be investigated. More importantly, one can note that these interactions are clearly limited when the sequence is optimized by our algorithm. Finally, a pronounced and rapid aggregation is observed when the nanoparticles are functionalized with complementary DNA strands, optimized or not. The aggregation regime differs according to the nature of the sequence, with faster kinetics observed when the sequence is optimized. More precisely, the hydrodynamic diameter increases from 250 nm to 1.5 μm after 1 hour 30 minutes of aggregation with optimized strands compared with 1.2 μm with nonoptimized ones. More information is available in [89] on the nature of the nonspecific interaction, reversibility of the assembly, overall kinetics, and role of temperature and salt concentration.

1.5.3 Structural and Energetic Properties of the Al/CuO Bionanocomposite

This last section evaluates the energy performance of nanobiocomposites described above. After evaporation of the solvent in a vacuum chamber for a few hours and drying, the aggregates are recovered and analyzed by differential scanning calorimetry (DSC) to measure the exothermic and endothermic reactions with respect to changes in temperature. The dried Al-CuO nanobiocomposite is placed in a platinum DSC crucible. A similar but empty crucible is also considered for reference. The heat exchanges between the sample and the reference are measured under a temperature ramp of 10 °C/min from 30 to 700 °C under an inert atmosphere (99.999% pure Ar). This characterization method is conventionally used for the analysis of nanothermite material reactions [91–94].

In Figure 1.23, we show the distinct DSC signatures of three different nanocomposites differing in their assembly protocols:

1) Assembly of functionalized Al and CuO nanoparticles with optimized and complementary DNA strands (blue curve).

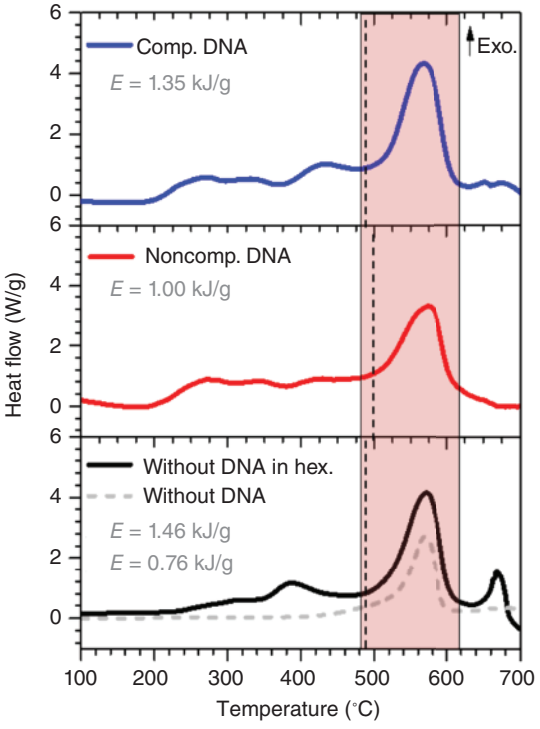

Figure 1.23 DSC curves of different Al-CuO nanobiocomposites obtained by assembly of Al and CuO nanoparticles with optimized and complementary DNA strands (blue curve), optimized and noncomplementary DNA strands (red curve), and noncomplementary functionalized DNA strands in aqueous solution (black curve) or in hexane (dashed grey curve).

2) Assembly of functionalized Al and CuO nanoparticles with optimized but non-complementary DNA strands (red curve).
3) Assembly of Al and CuO nanoparticles without DNA functionalization, mixed in aqueous solution (black curve) or in hexane-based organic solution (dashed gray curve).

The reaction enthalpies are annotated in the graphs, obtained from the area under the curve between 480 and 620 °C, highlighted by the colored zone.

First, the three curves have a similar profile. Some exothermic peaks are detected from 200 °C, which are associated with pollutants related to the ionic aqueous solvent used for the aggregation of particles. Then, the primary exothermic peak is centered at 570 °C for the three nanocomposites. Finally, the initiation temperature, corresponding to the beginning of the reaction and highlighted in dashed lines in Figure 1.23, is located at approximately 490 °C. Nanocomposites obtained from the aggregation of nanoparticles without DNA functionalization in aqueous solution and from the assembly of nanoparticles functionalized with complementary DNA strands initiated at a lower temperature than when the DNA strands were not complementary (490 versus 500 °C). Also, the reaction enthalpies were also the highest observed at 1.46 and 1.35 kJ/g, respectively. Composites obtained by assembling functionalized nanoparticles with noncomplementary DNA strands are significantly less efficient, with an enthalpy of 1.00 kJ/g. Finally, note that the nanocomposites generated in hexane, corresponding to the most commonly used method in

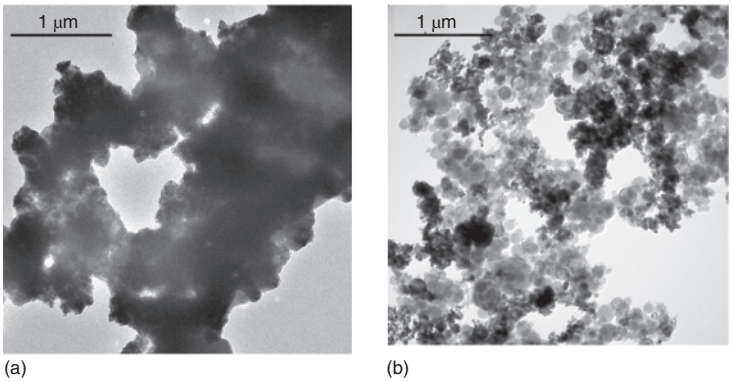

Figure 1.24 TEM images of nanocomposites made by direct mixing of Al and CuO nanoparticles (a) and assembled with optimized and complementary DNA strands (b).

the literature, have a much lower initiation temperature at approximately 440 °C but a low reaction enthalpy at 0.76 kJ/g. These results confirm the contribution of DNA in the nanostructuring of Al-CuO aggregates, as evidenced by the 135% increase in reaction enthalpy when the DNA strands are complementary. Thus, DNA has a notable impact in the organization of nanoparticles, which was further on confirmed by structural and chemical analysis. Figure 1.24 presents transmission electron microscopy (TEM) images that allow for direct comparisons between aggregates assembled through DNA or without.

The nanocomposite without DNA indeed appears much thicker than that made with complementary DNA strands, which appears spread on the surface. There are also clear geometric patterns in the first case, revealing the presence of NaCl crystals, which are not present in the nanobiocomposite. This greater thickness in the case of the nanocomposite without DNA shows that the aggregation of particles is equivalent in all spatial directions, retaining this structure at the time of drying.

The energy-dispersive X-ray spectroscopy (EDX) analysis in HR-TEM of these two powders, presented in Figure 1.25, confirms that the aggregation processes differs in both cases.

The presence of chlorine in the nanocomposite without DNA clearly validates the presence of NaCl crystals as previously presupposed. Notably, the distribution of Al and Cu is highly homogenous, with observed alterations in structural domains between 200 and 500 nm. However, the NaCl crystals are completely absent from the nanobiocomposite, and the DNA assembly exhibits slightly greater homogeneity.

These results enable an understanding of how the nanocomposite is organized during aggregation and especially drying. When there is no DNA to direct the placement of particles, the organization is random and occurs around NaCl crystals during their formation at the time of drying. If the amount of NaCl is sufficiently low, we have shown that the interaction between the particles is good and their alteration is highly homogenous, leading to higher thermal properties.

In contrast, when particles are functionalized with DNA, their assembly in aqueous solution is directed and optimized. At the time of drying, the composite is already

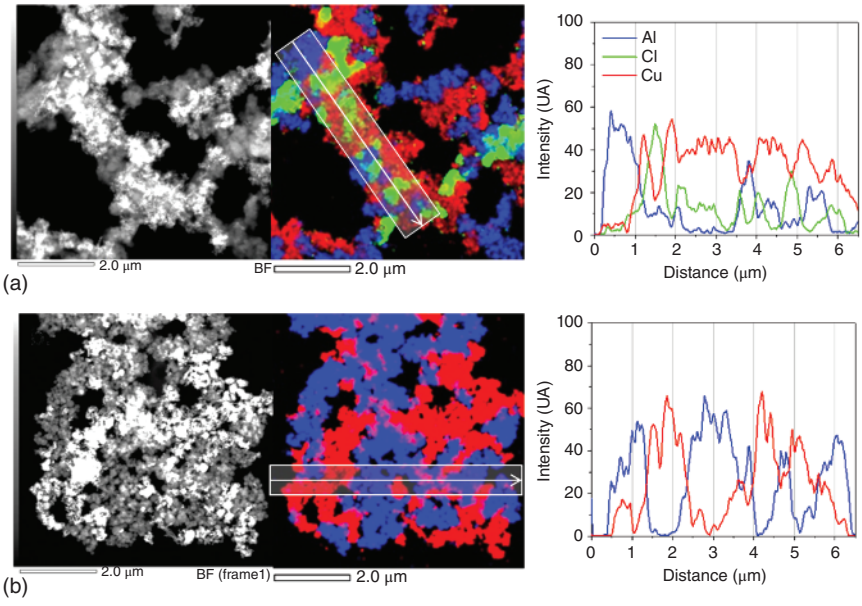

Figure 1.25 Dark-field TEM images: elemental maps of Al (blue), Cu (red), and Cl (green) and elemental composition of a slice of Al-CuO nanocomposites obtained by aggregation of Al and CuO nanoparticles without DNA (a) and by assembly with optimized and complementary DNA strands (b).

created, and NaCl does not crystallize within the material. The energy performances are also very good, thanks to a strong association of the particles and a highly homogeneous distribution. Importantly, DNA processing ensures a good reproducibility in the measured reaction enthalpies, with an average result of 1.25 ± 0.05 kJ/g obtained from four distinct samples. This is not the case in the experiments performed without DNA, for which large discrepancies were observed.

Finally, the low energetic performance of the composite made in hexane is explained by a very poor distribution of Al and CuO nanoparticles, pointing to the beneficial role of DNA-directed assembly. The TEM observations and EDX analysis results of these aggregates indeed show large clusters of CuO (between 0.5 and 1.5 µm in diameter) and a much lower Al level (75% CuO and 25% Al).

1.6 Conclusion

All the advances described in this review demonstrate the power and versatility of DNA nanotechnology to control the structuring of materials at the nanoscale. More than 30 years after suggesting the principle of using DNA as a tool dedicated to nanoconstruction, major advances have been reported in multiple directions. Among them, the assembly of nanoparticles has become a mainstream aspect of DNA nanotechnology, which again has demonstrated the potential to propose advanced and multifunctional materials that would not otherwise exist:

crystallization of an assembly of particles, nanoparticle decoration of functional superstructures, etc. This review describes the existing research efforts to integrate DNA nanotechnologies with nanoparticles. We further focused on one example application, namely, Al/CuO nanoparticle assembly, within a literature context dominated by pure metallic nanoparticle manipulation. This example also allowed us to expose key parameters and technological methodologies, making use of both experiment and theory, to optimize DNA-directed assembly as a route to move from laboratory proof of principle to more applied if not industrial processes. In particular, we highlighted the use of atomically precise techniques to evaluate fundamental interactions, demonstrating their multilevel complexity, including nonspecific to specific DNA interactions, grafting strategies, hybridization optimization and coding sequence choice. In this respect, we provided methodologies to quantify the performances of DNA-mediated grafting strategies. Finally, we discussed the assembly performance in the specific scope of an application dedicated to energetic nanomaterials.

Indeed, on the long term, the prospects for mass production must be considered. There are still many limiting factors due to scaling issues and the time and cost of manufacturing materials. From a functional point of view, the robustness, aging, performance, and design complexity of such materials must be further evaluated. Nevertheless, all the efforts made by research teams pave the way for DNA-based manufacturing of future generation of multifunctional materials.

References

1 Semiconductors, I. I. T. R. f. http://www.itrs.net.
2 Lehn, J.M. (1990). Perspectives in supramolecular chemistry – from molecular recognition towards molecular information-processing and self-organization. *Angew. Chem. Int. Ed.* 29 (11): 1304–1319.
3 Lehn, J.M. (1988). Supramolecular chemistry – scope and perspectives molecules, supermolecules, and molecular devices. *Angew. Chem. Int. Ed.* 27 (1): 89–112.
4 Thorkelsson, K., Bai, P., and Xu, T. (2015). Self-assembly and applications of anisotropic nanomaterials: a review. *Nano Today* 10 (1): 48–66.
5 Shimomura, M. and Sawadaishi, T. (2001). Bottom-up strategy of materials fabrication: a new trend in nanotechnology of soft materials. *Curr. Opin. Colloid Interface Sci.* 6 (1): 11–16.
6 Mastrangeli, M., Abbasi, S., Varel, C. et al. (2009). Self-assembly from milli-to nanoscales: methods and applications. *J. Micromech. Microeng.* 19 (8): 1–37.
7 Seeman, N.C. (1982). Nucleic-acid junctions and lattices. *J. Theor. Biol.* 99 (2): 237–247.
8 Seeman, N.C. (2003). DNA in a material world. *Nature* 421 (6921): 427–431.
9 Jones, M.R., Seeman, N.C., and Mirkin, C.A. (2015). Programmable materials and the nature of the DNA bond. *Science* 347 (6224): 1260901-1–1260901-11.

10 Service, R.F. (2011). DNA nanotechnology grows up. *Science* 332 (6034): 1140–1142.

11 Linko, V. and Dietz, H. (2013). The enabled state of DNA nanotechnology. *Curr. Opin. Biotechnol.* 24 (4): 555–561.

12 Sanchez, C., Belleville, P., Popall, M., and Nicole, L. (2011). Applications of advanced hybrid organic-inorganic nanomaterials: from laboratory to market. *Chem. Soc. Rev.* 40 (2): 696–753.

13 Hanus, M.J. and Harris, A.T. (2013). Nanotechnology innovations for the construction industry. *Prog. Mater Sci.* 58 (7): 1056–1102.

14 Rothemund, P.W.K. (2006). Folding DNA to create nanoscale shapes and patterns. *Nature* 440 (7082): 297–302.

15 Lu, Y. and Liu, J.W. (2006). Functional DNA nanotechnology: emerging applications of DNAzymes and aptamers. *Curr. Opin. Biotechnol.* 17 (6): 580–588.

16 Mirkin, C.A., Letsinger, R.L., Mucic, R.C., and Storhoff, J.J. (1996). A DNA-based method for rationally assembling nanoparticles into macroscopic materials. *Nature* 382 (6592): 607–609.

17 Reishus, D., Shaw, B., Brun, Y. et al. (2005). Self-assembly of DNA double-double crossover complexes into high-density, doubly connected, planar structures. *J. Am. Chem. Soc.* 127 (50): 17590–17591.

18 Zhang, J.P., Liu, Y., Ke, Y.G., and Yan, H. (2006). Periodic square-like gold nanoparticle arrays templated by self-assembled 2D DNA nanogrids on a surface. *Nano Lett.* 6 (2): 248–251.

19 Andersen, E.S., Dong, M., Nielsen, M.M. et al. (2009). Self-assembly of a nanoscale DNA box with a controllable lid. *Nature* 459 (7243): 73–U75.

20 Winfree, E., Liu, F.R., Wenzler, L.A., and Seeman, N.C. (1998). Design and self-assembly of two-dimensional DNA crystals. *Nature* 394 (6693): 539–544.

21 Liu, F.R., Sha, R.J., and Seeman, N.C. (1999). Modifying the surface features of two-dimensional DNA crystals. *J. Am. Chem. Soc.* 121 (5): 917–922.

22 Li, X.J., Yang, X.P., Qi, J., and Seeman, N.C. (1996). Antiparallel DNA double crossover molecules as components for nanoconstruction. *J. Am. Chem. Soc.* 118 (26): 6131–6140.

23 LaBean, T.H., Yan, H., Kopatsch, J. et al. (2000). Construction, analysis, ligation, and self-assembly of DNA triple crossover complexes. *J. Am. Chem. Soc.* 122 (9): 1848–1860.

24 Liu, D., Park, S.H., Reif, J.H., and LaBean, T.H. (2004). DNA nanotubes self-assembled from triple-crossover tiles as templates for conductive nanowires. *Proc. Natl. Acad. Sci. U.S.A* 101 (3): 717–722.

25 Liu, Y., Lin, C.X., Li, H.Y., and Yan, H. (2005). Protein nanoarrays – aptamer-directed self-assembly of protein arrays on a DNA nanostructure. *Angew. Chem. Int. Ed.* 44 (28): 4333–4338.

26 Shen, Z.Y., Yan, H., Wang, T., and Seeman, N.C. (2004). Paranemic crossover DNA: a generalized Holliday structure with applications in nanotechnology. *J. Am. Chem. Soc.* 126 (6): 1666–1674.

27 Yan, H., Zhang, X.P., Shen, Z.Y., and Seeman, N.C. (2002). A robust DNA mechanical device controlled by hybridization topology. *Nature* 415 (6867): 62–65.

28 Alivisatos, A.P., Johnsson, K.P., Peng, X.G. et al. (1996). Organization of 'nanocrystal molecules' using DNA. *Nature* 382 (6592): 609–611.

29 Condon, A. (2006). Designed DNA molecules: principles and applications of molecular nanotechnology. *Nat. Rev. Genet.* 7 (7): 565–575.

30 Vericat, C., Vela, M.E., Corthey, G. et al. (2014). Self-assembled monolayers of thiolates on metals: a review article on sulfur-metal chemistry and surface structures. *RSC Adv.* 4 (53): 27730–27754.

31 Calais, T., Bourrier, D., Bancaud, A. et al. (2017). DNA grafting and arrangement on oxide surfaces for self-assembly of Al and CuO nanoparticles. *Langmuir* 33 (43): 12193–12203.

32 Green, N.M. (1990). Avidin and streptavidin. *Methods Enzymol.* 184: 51–67.

33 Cobbe, S., Connolly, S., Ryan, D. et al. (2003). DNA-controlled assembly of protein-modified gold nanocrystals. *J. Phys. Chem. B* 107 (2): 470–477.

34 Zhang, Y.G., Lu, F., Yager, K.G. et al. (2013). A general strategy for the DNA-mediated self-assembly of functional nanoparticles into heterogeneous systems. *Nat. Nanotechnol.* 8 (11): 865–872.

35 Castelino, K., Kannan, B., and Majumdar, A. (2005). Characterization of grafting density and binding efficiency of DNA and proteins on gold surfaces. *Langmuir* 21 (5): 1956–1961.

36 Herne, T.M. and Tarlov, M.J. (1997). Characterization of DNA probes immobilized on gold surfaces. *J. Am. Chem. Soc.* 119 (38): 8916–8920.

37 Hurst, S.J., Lytton-Jean, A.K.R., and Mirkin, C.A. (2006). Maximizing DNA loading on a range of gold nanoparticle sizes. *Anal. Chem.* 78 (24): 8313–8318.

38 Blythe, K.L. and Willets, K.A. (2016). Super-resolution imaging of fluorophore-labeled DNA bound to gold nanoparticles: a single-molecule, single-particle approach. *J. Phys. Chem. C* 120 (2): 803–815.

39 Park, S.Y., Lytton-Jean, A.K.R., Lee, B. et al. (2008). DNA-programmable nanoparticle crystallization. *Nature* 451 (7178): 553–556.

40 Nykypanchuk, D., Maye, M.M., van der Lelie, D., and Gang, O. (2008). DNA-guided crystallization of colloidal nanoparticles. *Nature* 451 (7178): 549–552.

41 Demers, L.M., Mirkin, C.A., Mucic, R.C. et al. (2000). A fluorescence-based method for determining the surface coverage and hybridization efficiency of thiol-capped oligonucleotides bound to gold thin films and nanoparticles. *Anal. Chem.* 72 (22): 5535–5541.

42 Park, S.J., Lazarides, A.A., Storhoff, J.J. et al. (2004). The structural characterization of oligonucleotide-modified gold nanoparticle networks formed by DNA hybridization. *J. Phys. Chem. B* 108 (33): 12375–12380.

43 Hill, H.D., Macfarlane, R.J., Senesi, A.J. et al. (2008). Controlling the lattice parameters of gold nanoparticle FCC crystals with duplex DNA linkers. *Nano Lett.* 8 (8): 2341–2344.

44 Macfarlane, R.J., Jones, M.R., Senesi, A.J. et al. (2010). Establishing the design rules for DNA-mediated colloidal crystallization. *Angew. Chem. Int. Ed.* 49 (27): 4589–4592.

45 Xiong, H.M., van der Lelie, D., and Gang, O. (2009). Phase behavior of nanoparticles assembled by DNA linkers. *Phys. Rev. Lett.* 102 (1): 015504-1–015504-4.

46 Maye, M.M., Kumara, M.T., Nykypanchuk, D. et al. (2010). Switching binary states of nanoparticle superlattices and dimer clusters by DNA strands. *Nat. Nanotechnol.* 5 (2): 116–120.

47 Seo, S.E., Wang, M.X., Shade, C.M. et al. (2016). Modulating the bond strength of DNA-nanoparticle superlattices. *ACS Nano* 10 (2): 1771–1779.

48 Vo, T., Venkatasubramanian, V., Kumar, S. et al. (2015). Stoichiometric control of DNA-grafted colloid self-assembly. *Proc. Natl. Acad. Sci. U.S.A* 112 (16): 4982–4987.

49 Jin, R.C., Wu, G.S., Li, Z. et al. (2003). What controls the melting properties of DNA-linked gold nanoparticle assemblies? *J. Am. Chem. Soc.* 125 (6): 1643–1654.

50 Macfarlane, R.J., Lee, B., Hill, H.D. et al. (2009). Assembly and organization processes in DNA-directed colloidal crystallization. *Proc. Natl. Acad. Sci. U.S.A* 106 (26): 10493–10498.

51 Auyeung, E., Li, T.I.N.G., Senesi, A.J. et al. (2014). DNA-mediated nanoparticle crystallization into Wulff polyhedra. *Nature* 505 (7481): 73–77.

52 Auyeung, E., Macfarlane, R.J., Choi, C.H.J. et al. (2012). Transitioning DNA-engineered nanoparticle superlattices from solution to the solid state. *Adv. Mater.* 24 (38): 5181–5186.

53 De Stefano, M. and Gothelf, K.V. (2016). Dynamic chemistry of disulfide terminated oligonucleotides in duplexes and double-crossover tiles. *ChemBioChem* 17 (12): 1122–1126.

54 Lermusiaux, L., Sereda, A., Portier, B. et al. (2012). Reversible switching of the interparticle distance in DNA-templated gold nanoparticle dimers. *ACS Nano* 6 (12): 10992–10998.

55 Lermusiaux, L. and Bidault, S. (2015). Increasing the morphological stability of DNA-templated nanostructures with surface hydrophobicity. *Small* 11 (42): 5696–5704.

56 Severac, F., Alphonse, P., Esteve, A. et al. (2012). High-energy Al/CuO nanocomposites obtained by DNA-directed assembly. *Adv. Funct. Mater.* 22 (2): 323–329.

57 Fan, J.A., He, Y., Bao, K. et al. (2011). DNA-enabled self-assembly of plasmonic nanoclusters. *Nano Lett.* 11 (11): 4859–4864.

58 Tan, L.H., Xing, H., Chen, H.Y., and Lu, Y. (2013). Facile and efficient preparation of anisotropic DNA-functionalized gold nanoparticles and their regioselective assembly. *J. Am. Chem. Soc.* 135 (47): 17675–17678.

59 Cederquist, K.B. and Keating, C.D. (2009). Curvature effects in DNA: Au nanoparticle conjugates. *ACS Nano* 3 (2): 256–260.

60 Xing, H., Wang, Z.D., Xu, Z.D. et al. (2012). DNA-directed assembly of asymmetric nanoclusters using Janus nanoparticles. *ACS Nano* 6 (1): 802–809.

61 Jones, M.R., Macfarlane, R.J., Lee, B. et al. (2010). DNA-nanoparticle superlattices formed from anisotropic building blocks. *Nat. Mater.* 9 (11): 913–917.

62 Macfarlane, R.J., Lee, B., Jones, M.R. et al. (2011). Nanoparticle superlattice engineering with DNA. *Science* 334 (6053): 204–208.
63 Millstone, J.E., Georganopoulou, D.G., Xu, X.Y. et al. (2008). DNA-gold triangular nanoprism conjugates. *Small* 4 (12): 2176–2180.
64 Knorowski, C. and Travesset, A. (2014). Self-assembly and crystallization of hairy (f-Star) and DNA-grafted nanocubes. *J. Am. Chem. Soc.* 136 (2): 653–659.
65 Macfarlane, R.J., Jones, M.R., Lee, B. et al. (2013). Topotactic interconversion of nanoparticle superlattices. *Science* 341 (6151): 1222–1225.
66 Valignat, M.P., Theodoly, O., Crocker, J.C. et al. (2005). Reversible self-assembly and directed assembly of DNA-linked micrometer-sized colloids. *Proc. Natl. Acad. Sci. U.S.A* 102 (12): 4225–4229.
67 Biancaniello, P.L., Crocker, J.C., Hammer, D.A., and Milam, V.T. (2007). DNA-mediated phase behavior of microsphere suspensions. *Langmuir* 23 (5): 2688–2693.
68 Geerts, N., Schmatko, T., and Eiser, E. (2008). Clustering versus percolation in the assembly of colloids coated with long DNA. *Langmuir* 24 (9): 5118–5123.
69 Biancaniello, P.L., Kim, A.J., and Crocker, J.C. (2005). Colloidal interactions and self-assembly using DNA hybridization. *Phys. Rev. Lett.* 94 (5).
70 Kim, A.J., Biancaniello, P.L., and Crocker, J.C. (2006). Engineering DNA-mediated colloidal crystallization. *Langmuir* 22 (5): 1991–2001.
71 Kim, A.J., Scarlett, R., Biancaniello, P.L. et al. (2009). Probing interfacial equilibration in microsphere crystals formed by DNA-directed assembly. *Nat. Mater.* 8 (1): 52–55.
72 Di Michele, L. and Eiser, E. (2013). Developments in understanding and controlling self assembly of DNA-functionalized colloids. *Phys. Chem. Chem. Phys.* 15 (9): 3115–3129.
73 Wang, Y.F., Wang, Y., Zheng, X.L. et al. (2015). Synthetic sstrategies toward DNA-coated colloids that crystallize. *J. Am. Chem. Soc.* 137 (33): 10760–10766.
74 Zhou, C., Duan, X.Y., and Liu, N. (2017). DNA-nanotechnology-enabled chiral plasmonics: from static to dynamic. *Acc. Chem. Res.* 50 (12): 2906–2914.
75 Liu, J.W. and Lu, Y. (2006). Fast colorimetric sensing of adenosine and cocaine based on a general sensor design involving aptamers and nanoparticles. *Angew. Chem. Int. Ed.* 45 (1): 90–94.
76 Lee, J.S., Ulmann, P.A., Han, M.S., and Mirkin, C.A. (2008). A DNA-gold nanoparticle-based colorimetric competition assay for the detection of cysteine. *Nano Lett.* 8 (2): 529–533.
77 Pavlov, V., Xiao, Y., Shlyahovsky, B., and Willner, I. (2004). Aptamer-functionalized Au nanoparticles for the amplified optical detection of thrombin. *J. Am. Chem. Soc.* 126 (38): 11768–11769.
78 Rosi, N.L. and Mirkin, C.A. (2005). Nanostructures in biodiagnostics. *Chem. Rev.* 105 (4): 1547–1562.
79 Bruchez, M., Moronne, M., Gin, P. et al. (1998). Semiconductor nanocrystals as fluorescent biological labels. *Science* 281 (5385): 2013–2016.

80 Auyeung, E., Morris, W., Mondloch, J.E. et al. (2015). Controlling structure and porosity in catalytic nanoparticle superlattices with DNA (vol 137, pg 1658, 2015). *J. Am. Chem. Soc.* 137 (11): 3993–3993.

81 Son, S.F., Asay, B.W., Foley, T.J. et al. (2007). Combustion of nanoscale Al/MoO_3 thermite in microchannels. *J. Propul. Power* 23 (4): 7.

82 Schoenitz, M., Umbrajkar, S., and Dreizin, E.L. (2007). Kinetic analysis of thermite reactions in Al-MoO_3 nanocomposites. *J. Propul. Power* 23 (4): 5.

83 Sanders, E.V., Asay, B.W., Foley, T.J. et al. (2007). Reaction propagation of four nanoscale energetic composites (Al/MoO_3, Al/WO_3, Al/CuO, and Bi_2O_3). *J. Propul. Power* 23 (4): 8.

84 Foley, T., Pacheco, A., Malchi, J. et al. (2007). Development of nanothermite composites with variable electrostatic discharge ignition thresholds. *Propellants Explos. Pyrotech.* 32 (6): 431–434.

85 Pantoya, M.L. and Granier, J.J. (2006). The effect of slow heating rates on the reaction mechanisms of nano and micron composite thermite reactions. *J. Therm. Anal. Calorim.* 85 (1): 37–43.

86 Bockmon, B.S., Pantoya, M.L., Son, S.F. et al. (2005). Combustion velocities and propagation mechanisms of metastable interstitial composites. *J. Appl. Phys.* 98 (6): 064903–064907.

87 Calais, T., Playe, B., Ducere, J.M. et al. (2015). Role of alumina coatings for selective and controlled bonding of DNA on technologically relevant oxide surfaces. *J. Phys. Chem. C* 119 (41): 23527–23543.

88 Cutler, J.I., Auyeung, E., and Mirkin, C.A. (2012). Spherical nucleic acids. *J. Am. Chem. Soc.* 134 (3): 1376–1391.

89 Calais, T., Baijot, V., Rouhani, M.D. et al. (2016). General strategy for the design of DNA coding sequences applied to nanoparticle assembly. *Langmuir* 32 (37): 9676–9686.

90 SantaLucia, J. and Hicks, D. (2004). The thermodynamics of DNA structural motifs. *Annu. Rev. Biophys. Biom.* 33: 415–440.

91 Sun, J., Pantoya, M.L., and Simon, S.L. (2006). Dependence of size and size distribution on reactivity of aluminum nanoparticles in reactions with oxygen and MoO_3. *Thermochim. Acta* 444 (2): 117–127.

92 Stamatis, D., Jiang, Z., Hoffmann, V. et al. (2009). Fully dense, aluminum-rich Al-CuO nanocomposite powders for energetic formulations. *Combust. Sci. Technol.* 181 (1): 97–116.

93 Bahrami, M., Taton, G., Conedera, V. et al. (2014). Magnetron sputtered Al-CuO nanolaminates: effect of stoichiometry and layers thickness on energy release and burning rate. *Propellants Explos. Pyrotech.* 39 (3): 365–373.

94 Glavier, L., Taton, G., Ducere, J.M. et al. (2015). Nanoenergetics as pressure generator for nontoxic impact primers: comparison of Al/$Bi2O_3$, Al/CuO, Al/MoO_3 nanothermites and Al/PTFE. *Combust. Flame* 162 (5): 1813–1820.